MARS CLIMATE DATABASE v4.3
DETAILED DESIGN DOCUMENT

(ESTEC Contract 11369/95/NL/JG)

CNES Contract "Base de données climatique martienne"

E. Millour, F. Forget (LMD) and S.R. Lewis (OU)

May 2008

Abstract

This is the Detailed Design Document for version 4.3 of the Mars Climate Database (MCD) and replaces previous versions which described earlier versions (1.0, 2.x and 3.x) of the database. It updates (and reproduces, when still relevant) material from previous Detailed Design Documents and also covers new features.
This document contains a detailed description of the database and addresses technical aspects of how the data is represented, manipulated and post-processed by the MCD access software.
Instructions on how to install the MCD and use the provided access software and post-processing tools are given in the MCD v4.3 **User Manual**. Comparisons of MCD outputs with available measurements are given in the MCD v4.3 **Validation Document**.

Contents

1 Introduction

The Mars Climate Database (MCD) is a database of atmospheric statistics compiled from state-of-the art General Circulation Model (GCM) simulations of the Martian atmosphere (Forget et al., 1999). The models used to compile the statistics have been extensively validated using available observational data and represent the current best knowledge of the state of the Martian atmosphere given the observations and the physical laws which govern the atmospheric circulation and surface conditions on the planet.

This document provides the user of the MCD with a detailed description of the database structure and of technical aspects of the access software.

The MCD is freely available on DVD, and an up-to-date copy of its contents (excluding the data files) is always available on line at:
`http://www.lmd.jussieu.fr/~forget/dvd/`
(see the `README` file there for details of minor enhancements and additions that may have been performed since the delivery of your copy).

Note that the MCD may also be accessed (in a more limited form than with the access software of the DVD) using a Live Access Server on our WWW site at:
`http://www-mars.lmd.jussieu.fr`

2 Differences Between Version 4.3 and Previous Versions of the MCD

Differences between version 4.3 and version 4.2

- The main upgrade in MCD version 4.3 is the improvement of the large scale perturbation model. Version 4.3 thus uses the same database datafiles as version 4.2, except for a subset which contains updated data required for the large scale perturbation model.
- Other changes that have been introduced are:
  - An additional vertical coordinate ('zkey' parameter) may be used to specify vertical coordinate as altitude above reference radius (arbitrarily set to 3.39610^6 m).
  - The output unit to which messages are written is now a parameter that can be set by the user (the default output unit is set to 6, which implies, in conformance with Fortran standards, the standard output).

Differences between version 4.2 and version 4.1

- Version 4.2 uses the same database datafiles as version 4.1, except for a small subset (the files which contain variability); most improvements, changes and new features are in the access and postprocessing software.
- The main new features and differences are:
  1. The main Fortran subroutine to retrieve data from the database is now called "call_mcd" and **significant changes to the argument list**, compared to its predecessor "atmemcd", have been introduced:
     - A new high resolution procedure (based on the integration of high resolution 32 pixels per degree MOLA topography) has been implemented.
     - Input and output arguments which are floating numbers are now declared as **single precision** (i.e. Fortran REAL), except 'xdate', which is double precision, (i.e. Fortran REAL*8).

- The way by which users impose date and local time has changed.
- Input **longitude and latitude must now be given in degrees**. Longitude is interpreted as degrees east (as before).
- Input arguments used to signal and generate perturbations have been changed.
- Day to day variability of atmospheric variables is now given either pressure-wise or altitude-wise, depending on the vertical coordinate selected by the user.

2. Examples of interface software for C, C++ and Scilab users, have been added (in addition to the pre-existing IDL and Matlab ones).
3. Computation of solar longitude (from a given Julian date) has been made more accurate. Computation of local time (given in true solar time) has been improved by using an appropriate equation of time.
4. The "pres0" tool has been updated.

Lists of changes and improvements of previous versions of the MCD

- Version 4.1 is similar to beta version 4.0 with some improvements and a few problems fixed.
- The main differences between version 4 and previous version 3.1 are:

1. The database now extends up to the thermosphere and new variables (upper atmospheric composition: CO_2, N_2, CO, O, H_2 and, in the lower atmosphere: water, water ice, ozone, dust) are available.
2. Different vertical coordinates may be specified as input, including pressure level.
3. A linear interpolation in time (Ls) for mean variables between seasons was added.
4. For some variables, an estimation of the "day to day" variation is provided (root mean square values).
5. There is a significant re-arrangement of arguments of atmemcd so that all the input variables are followed by all the output variables.
6. We suggest the use of direct compilation rather than using the UNIX command "make".
7. Variables are now saved in atmemcd to fix problems with F77 compilers which don't store values of variables between subroutine calls.
8. The database now has a more accurate representation of gravity; the fact that it varies following an inverse square law is accounted for when integrating the hydrostatic equation. The variation of R, the gas constant, with altitude is also taken into account.
9. The horizontal resolution of the database has changed to $5.625° \times 3.75°$ (longitude $\times$ latitude).
10. We now provide the separate tool to compute surface pressure with high accuracy.
11. We now provide some tool to use the database software from IDL.

- A major change in Version 3.1, compared to version 3.0 of the database, is the change from DRS data format to NetCDF. A bug was also fixed for the calculation of large scale variability in the upper atmosphere (above 120 km).
- The main differences between version 3.0 and 2.3 are mostly related to the content of the database files, due in particular to improvements made in the models used to build the database, including an extension of the model top from 80 to 120 km, improved surface properties and a dust scenarios from Mars Global Surveyor.

- The main difference between version 2.3 and 2.0 is the use of the main subroutine ATMEMCD which computes meteorological variables from the Mars Climate Database (MCD).
- The main difference between version 2.0 and 1.0 of the MCD is that the large-scale variability model now makes use of two-dimensional, multivariate Empirical Orthogonal Functions (EOFs). These now describe correlations in the model variability as a function of both height and longitude (rather than solely of height as in version 1.0).

3 General Description of Database Contents

3.1 MCD Files

The DVD contains three directories: `docs` which contains documentation, `data` which contains the datafiles and `mcd` which contains the access software.

3.2 MCD Software

Subdirectory `mcd` contains the following Fortran programs:

- `call_mcd.F`: This is the main subroutine which should be used to retrieve data from the database. The file also contains a collection of subsidiary routines. It requires the include file `constants_mcd.inc` to run and also uses subroutine `heights.F`. Input and output arguments of `call_mcd` are documented in the MCD User Guide.
- `heights.F`: This subroutine performs conversions between different height coordinates (namely altitude above local surface, above areoid or distance to the center of planet). It is used by `call_mcd.F` and has only been kept separate from the rest of the subroutines as a facility for some users.
- `julian.F`: A subroutine which converts Earth date into the corresponding Julian date (one of the forms of date input used by `call_mcd`).
- `test_mcd.F`: A sample program provided to display (and test) the way to call subroutine `call_mcd` and to retrieve data from the MCD.

The `pres0` subdirectory also contains a post-processing subroutine, `pres0.F`, which can be used to retrieve high resolution surface pressure. As of version 4.2 of the MCD, this feature is also implemented in `call_mcd`, which makes this utility redundant. It has however been retained in the MCD distribition for users who are only interested in retrieving high resolution surface pressure and require a minimal and light tool to do so.

Apart from these Fortran programs, the `mcd` directory also contains subdirectories whith examples of interfaces for other languages: `idl`, `matlab`, `scilab` and `c_intefaces` (which contains both C and C++ interface examples). See the acompanying `README` files and the MCD User Guide for details.

3.3 MCD Datasets and Datafiles

MCD data is stored in various files in directory `data` of the DVD, using the Network Common Data Form (NetCDF) developed and distributed by Unidata. The NetCDF libraries are freely available for numerous platforms from the Unidata web site:
`http://www.unidata.ucar.edu/software/netcdf`

Mean variable	symbol	units	2-D or 3-D
CO_2 ice cover	co2ice	kg m^{-2}	2-D
Surface temperature	tsurf	K	2-D
Surface pressure	ps	Pa	2-D
LW (thermal IR) radiative flux to surface	fluxsurf_lw	W m^{-2}	2-D
SW (solar) radiative flux to surface	fluxsurf_sw	W m^{-2}	2-D
LW (thermal IR) radiative flux to space	fluxtop_lw	W m^{-2}	2-D
SW (solar) radiative flux to space	fluxtop_sw	W m^{-2}	2-D
Dust optical depth	dod		2-D
Water vapor column	col_h2ovapor	kg m^{-2}	2-D
Water ice column	col_h2oice	kg m^{-2}	2-D
Atmospheric temperature	temp	K	3-D
Zonal (Eastward) wind	u	m s^{-1}	3-D
Meridional (Northward) wind	v	m s^{-1}	3-D
Vertical (downward) wind	w	m s^{-1}	3-D
Atmospheric density	rho	kg m^{-3}	3-D
Boundary layer eddy kinetic energy	q2	m^2 s^{-2}	3-D
Water vapor volume mixing ratio	vmr_h2ovapor	mol/mol	3-D
Water ice volume mixing ratio	vmr_h2oice	mol/mol	3-D
Ozone volume mixing ratio	vmr_o3	mol/mol	3-D

Table 1: Variables stored in database mean `me` data files.

The file naming convention of MCD datafiles is as follows: filenames are a concatenation of 3 to 5 keywords (separated by an underscore _) of the form `VVVV_WW_ZZ.nc` for lower atmosphere data, `VVVV_WW_thermo_XXX_ZZ.nc` for thermospheric data and `VVVV_all_XXX_eo.nc` for EOF data. The possible keywords and their meaning are:

- The first series of character (`VVVV`) denote the dust scenario the data corresponds to. It may be `MY24` for Mars Year 24, `cold` for clear atmosphere (dust opacity $\tau = 0.1$, topped by a solar EUV minimum thermosphere), `warm` for dusty atmosphere (topped by a solar EUV maximum thermosphere) or `strm` for dust storm (dust opacity set to $\tau = 4$)
- The second keyword (`WW`) indicates Mars month number, an integer ranging from `01` to `12` (EOF data span the year and so have `all` in place of `WW`).
- `ZZ` indicates the type of data in the file and may be either `me` to indecate mean data, `sd` for standard deviation statistics or `eo` for EOF data.
- Keyword `XXX`, only present for thermospheric datafiles, denotes the EUV scenario, which may be `min` for minimum, `ave` for average or `max` for maximum.

Hence file `MY24_04_me.nc` contains lower atmospheric mean data for the fourth month of the Mars Year 24 dust scenario.

Each of the `me` mean data files contain 12 mean values (for the given month) corresponding to 12 solar times of day (i.e. every 2 hours) for the variables shown in Table 1. The `sd` data files contain day-to-day RMS values of variables (see Table 2 for details).

The EOF datafiles (`eo`) contain normalized, multi-dimensional EOFs of zonal wind, meridional wind, atmospheric temperature and surface pressure as well as some normalization factors, eigenvalues and principal component model coefficients. It is recommended that you use the software supplied to access and exploit the data in these files.

In addition to these datafiles, the `data` directory also contains the following files:

RMS of 2D variables	symbol	units
Surface temperature	rmstsurf	K
Surface pressure	rmsps	Pa
Dust optical depth	rmsdod	
Pressure-wise RMS of 3D variables	**symbol**	**units**
Atmospheric temperature	rmstemp	K
Zonal (Eastward) wind	rmsu	m s^{-1}
Meridional (Northward) wind	rmsv	m s^{-1}
Vertical (downward) wind	rmsw	m s^{-1}
Atmospheric density	rmsrho	kg m^{-3}
Altitude-wise RMS of 3D variables	**symbol**	**units**
Atmospheric temperature	armstemp	K
Zonal (Eastward) wind	armsu	m s^{-1}
Meridional (Northward) wind	armsv	m s^{-1}
Vertical (downward) wind	armsw	m s^{-1}
Atmospheric density	armsrho	kg m^{-3}
Atmospheric pressure	armspressure	Pa

Table 2: Day-to-day RMS of variables stored in database `sd` data files, which is, for 3D atmopsheric variables, given pressure-wise (i.e. evaluated at fixed pressure) and altitude-wise (i.e. evaluated at fixed altitude).

- File `mountain.nc` which contains maps (at model resolution, i.e. a 64x49 longitude-latitude grid) of topography, areoid and sub-gridscale standard deviation of topography (useful for computing gravity wave perturbations).
- File `mola32.nc` which contains a high resolution (32 pixels per degree) map of Martian topography.
- File `mgm1025` contains the spherical harmonic expansion coefficients necessary to compute the Martian areoid with high accuracy.
- File `VL1.ls` contains a diurnaly averaged and smoothed record of surface pressure at Viking Lander 1 site.
- File `ps_MY24.nc` contains a minimal subset of MCD data which is used by the standalone 'pres0' tool.

3.4 Database Grid Structure

3.4.1 Horizontal Structure

Variables in the database are stored on the grid on which they are obtained from the general circulation model (GCM) runs: a regular, equispaced horizontal 64×49 grid[1] in East longitude×latitude. Longitudes thus range from $-180.0°$ to $174.375°$ in steps of $5.625°$ and latitudes from $90°$ to $-90°$ in steps of $3.75°$.

Figure 1 displays the GCM horizontal grid.

[1]Technically, this grid is not exactly the computational grid: dynamical variables are in fact computed on a complementary staggered grid.

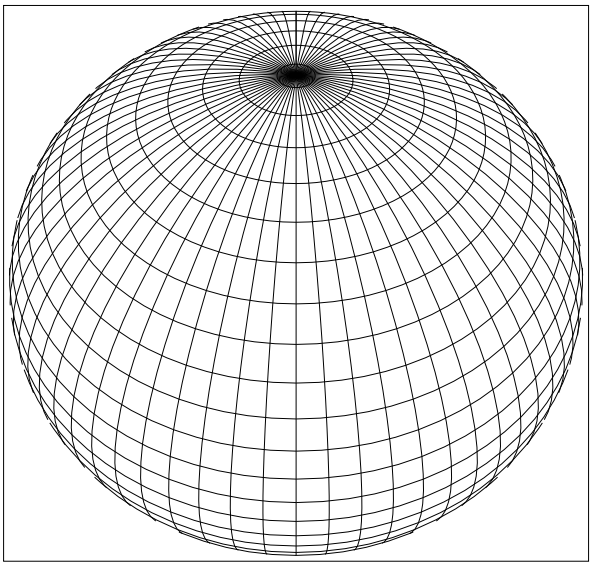

Figure 1: "Satellite" view (above latitude 60N) of the database grid, illustrating the regular equispaced horizontal grid and resulting decreasing mesh size toward the poles.

3.4.2 Vertical Structure

Variables in the database are stored on the same vertical grid on which they are computed. This vertical coordinate is a hybrid coordinate in which vertical levels l are at pressure P:

$$P(l) = aps(l) + bps(l).P_S \tag{1}$$

where P_S is surface pressure. Coefficients $aps(l)$ and $bps(l)$ are respectively hybrid pressure and hybrid sigma levels.
In its present form the database extends over 50 levels and variables in the datafiles are split between lower atmosphere ($l = 1, \ldots, 30$) and thermospheric ($l = 31, \ldots, 50$, for `thermo` datafiles). This is due to the fact that only the thermosphere is affected by solar EUV input, unlike the lower part of the atmosphere. In order to reconstruct a column of data, one must thus extract the first 30 levels from 'lower atmosphere' datafiles and obtain the following 20 from the corresponding 'thermosphere' datafiles.

Note that *aps* and *bps* are prescribed coefficients such that near the surface (small values of l) levels are essentialy terrain-following sigma coordinates, whereas at high altitude (large values of l) the vertical levels are pressure levels, as shown in Figure 2. Values of coefficients *aps* and *bps* are given in the following table, along with corresponding pseudo-altitude which are the approximative heights above local surface of the corresponding layer (computed using a surface pressure of 610 Pa and a scale height of 10 km; it is thus a rough estimate and particularly inaccurate in the upper atmosphere above 80 km because it does not account for actual changes in temperatures and scale height there).

Layer	hybrid pressure level aps (Pa)	hybrid sigma level bps	pseudo-altitude (km)
1	0.005627457	0.9994375	0.005534718
2	0.02046412	0.9979548	0.02013585
3	0.05033206	0.9949741	0.04955606
4	0.1184753	0.9881924	0.1168125
..... table continued next page			

Layer	hybrid pressure level aps (Pa)	hybrid sigma level bps	pseudo-altitude (km)
5	0.2561847	0.9745585	0.2533987
6	0.5133207	0.9493409	0.5110131
7	0.9835082	0.9039375	0.9921301
8	1.793413	0.8273973	1.859232
9	3.040181	0.7122511	3.323518
10	4.673814	0.5632383	5.605408
11	6.414024	0.4016031	8.864458
12	7.858505	0.2559445	13.13686
13	8.728997	0.1458385	18.31655
14	8.996318	0.0742123	24.19564
15	8.779466	0.03266766	30.56327
16	8.121207	0.01070902	37.28765
17	6.264208	0.001721705	44.23607
18	3.632228	$5.758683\ 10^{-8}$	51.23603
19	1.803712	$1.715984\ 10^{-30}$	58.23612
20	0.8956969	0	65.23612
21	0.44479	0	72.23612
22	0.2208762	0	79.23612
23	0.1096839	0	86.23612
24	0.05446739	0	93.23612
25	0.02704768	0	100.2361
26	0.01343142	0	107.2362
27	0.006669816	0	114.2362
28	0.003312133	0	121.2362
29	0.001644756	0	128.2362
30	0.0008167619	0	135.2362
31	0.0004055919	0	142.2362
32	0.000201411	0	149.2362
33	0.0001000177	0	156.2362
34	$4.966735\ 10^{-5}$	0	163.2362
35	$2.466407\ 10^{-5}$	0	170.2362
36	$1.224782\ 10^{-5}$	0	177.2362
37	$6.082086\ 10^{-6}$	0	184.2362
38	$3.020274\ 10^{-6}$	0	191.2362
39	$1.499824\ 10^{-6}$	0	198.2362
40	$7.447904\ 10^{-7}$	0	205.2362
41	$3.69852\ 10^{-7}$	0	212.2362
42	$1.83663\ 10^{-7}$	0	219.2362
43	$9.120437\ 10^{-8}$	0	226.2362
44	$4.529075\ 10^{-8}$	0	233.2362
45	$2.249072\ 10^{-8}$	0	240.2362
46	$1.116856\ 10^{-8}$	0	247.2362
47	$5.546143\ 10^{-9}$	0	254.2362
48	$2.754131\ 10^{-9}$	0	261.2362
49	$1.36766\ 10^{-9}$	0	268.2362
50	$6.791596\ 10^{-10}$	0	275.2362

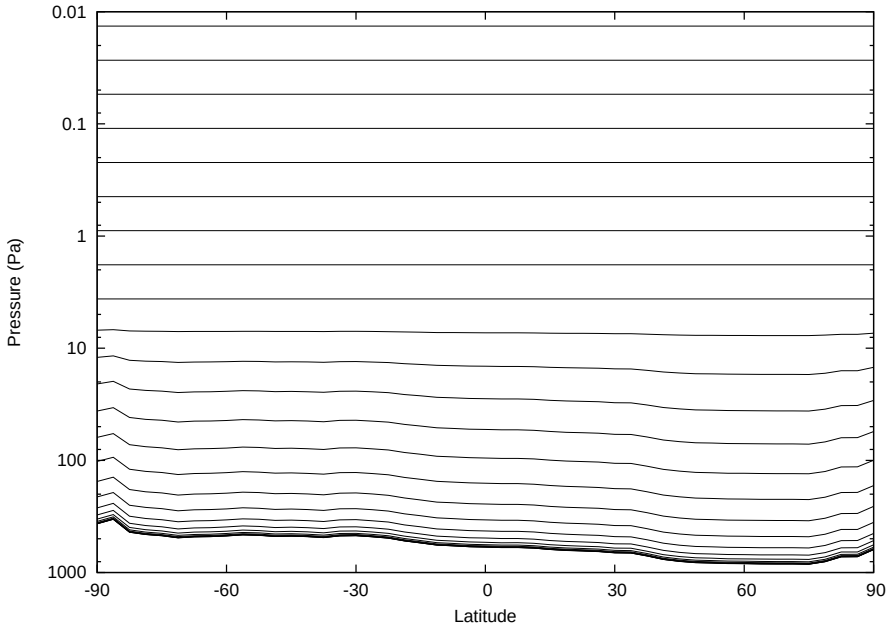

Figure 2: Illustration of the vertical hybrid coordinate: This plot displays the pressures at which the MCD vertical levels are located (slice of data taken at noon and longitude=0, at $Ls \simeq 195°$, i.e. the 7th month of the MY24 scenario). Note that only the first 26 levels are shown in order to show that near the surface levels are essentially terrain-following. The MCD vertical levels extend to much lower pressures, down to $P = 6.810^{-10}$ Pa for the last (fiftieth) level.

3.4.3 Temporal Structure

In order to store the seasonal behaviour of variables, data from the General Circulation Model was processed to be stored along 12 martian months. Each of these month is defined as spaning 30° in solar longitude (months are thus "centered" on solar longitudes $Ls = 15°$, $45°$, ...). Due to the eccentricity of Mars' orbit, martian months vary from 46 to 66 sols (martian solar days) long, as shown in Table 4.

Time evolution of variables on the scale of a sol is included in the datafiles where values at 12 times of day are stored. Martian hours are defined as being 1/24th of a sol. To avoid confusion, we do not use (or define) martian minutes or seconds: any martian time of day is always given as a fraction of a sol or in martian hours and decimal fractions thereof (e.g. $time = 18.5$ hours means 18 hours and a half).

The database reference time is Mars Universal Time (which is simply "prime meridian time", i.e. the local time at 0° longitude) and data is stored every 2 martian hours, i.e. from 2 to 24 hours. Note that all times are expressed in True Solar Time (the sun is highest at noon) and not Mean Solar Time (see the description of the Equation Of Time in Appendix A).

The Local True Solar Time $LTST$ at a given East longitude lon (expressed in degrees) may easily be computed from the Local True Solar Time at longitude zero $LTST_0$ (i.e. Mars Universal Time) by the following formula:

$$LTST = LTST_0 + lon/15 \tag{2}$$

Month number	Solar longitude range	Duration (in sols)
1	0 - 30	61
2	30 - 60	66
3	60 - 90	66
4	90 - 120	65
5	120 - 150	60
6	150 - 180	54
7	180 - 210	50
8	210 - 240	46
9	240 - 270	47
10	270 - 300	47
11	300 - 330	51
12	330 - 360	56

Table 4: Lenght of martian months. Note that a martian year is 668.6 sols (martian solar days) long and that a sol is 88775.245 seconds long; For convenience, the durations given above are rounded to be integer values.

4 Dust Distribution and EUV Scenarios in the MCD

Eight combinations of dust and and solar Extreme UltraViolet (EUV) scenarios are included in the MCD, as both of these forcings are highly variable from a year to another:

- The major factor which governs the variablity of the Martian atmosphere is the amount and distribution of suspended dust. Because of this variability, and since for a given year the details of the dust distribution and optical properties can be uncertain, multi-annual model integrations were carried out for the MCD assuming various "dust scenarios", i.e. prescribed amount of airborne dust in the simulated atmosphere. Of the four scenarios included in the MCD, one, the **Mars Year 24 (MY24)** dust scenario, is designed to mimic Mars as observed by Mars Global Surveyor from 1999 to June 2001[2], a martian year thought to be representative of one without a global dust storm. Two other dust scenarios, **cold** and **warm**, are provided to bracket the most likely global conditions on Mars, outside global dust storms. The later are represented as a separate **dust storm** scenario.

- At high altitudes (above roughly 120 km), the heating of the atmosphere is controled by the EUV input from the Sun, which varies significantly on an 11 year cycle. To account for the variability induced by the solar EUV input, simulated atmospheres obtained from concidering three corresponding EUV scenarios, **maximum**, **average** and **minimum** are provided.

How these dust and EUV scenarios are taken into account is detailed in the following subsections.

4.1 The EUV Scenarios

The radiative output of the Sun is known to vary at different timescales: for example, due to the solar flares (timescale of minutes to hours), to the solar rotation (27 days) or to the magnetic cycle of the Sun (11 years, the so-called solar cycle) (Tobiska, 2001; Woods *et al.*, 2004). This last variability, first detected counting the number of sunspots, is more

[2]This corresponds to the 24th martian year according to the calendar proposed by R. Todd Clancy (Clancy et al., *Journal of Geophys. Res* 105, p 9553, 2000) which starts (Ls=0°) on April 11, 1955.

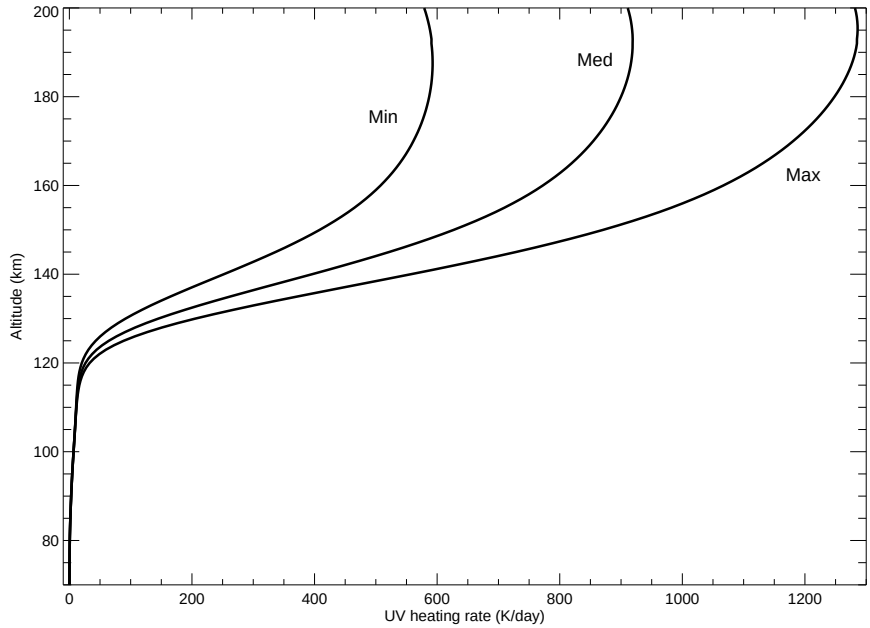

Figure 3: Illustration of the heating rates obtained by the photochemical model used in the simulations, for the solar EUV minimum (MIN), average (MED) and maximum (MAX) scenarios.

important in the UV (than in the visible) region of the solar spectrum, as a variability of about a factor 2 in the total EUV irradiance (below 120 nm) with the solar cycle is found (Woods *et al.*, 2004). Although the UV spectral region represents a small contribution to the total solar energy (Lean, 1987), the UV radiation is the major heating source of the Martian upper atmosphere (above about 120 km). So, its variability has a strong impact over the thermospheric temperatures (e.g. Banks and Kockarts, 1973).

Only the variation of the UV solar flux with the 11 year solar cycle is taken into account (the variability at other timescales, e.g. 27 days, has not be adressed so far) in the MCD, by including three solar EUV input scenarios. The "Solar maximum" scenario corresponds to the conditions when the solar is at its maximum activity (approximate value for F10.7[3] at Earth around 200) and the UV emission is highest. For such conditions, a rise in temperatures in the thermosphere, induced by a more intense UV heating, is expected (and obtained). On the opposite, the "Solar minimum" scenario is appropriate for conditions when the sun is at its minimum activity (approximate value of F10.7 at Earth around 70). In this case, UV emission is low, so a lower temperature due to a lower UV heating is expected. The "Solar average" scenario is an intermediate situation between maximum and minimum (approximate value for F10.7 at Earth 130) solar activity. Figure 3 displays heating rates corresponding the the three EUV scenarios and Figure 4 illustrates the impact of the solar EUV input on atmospheric temperature.

It has to be taken into account that the F10.7 values mentioned above for the different scenarios are only indicative, as this index is not used in the GCM as an indicator of the solar activity. Instead, a sinusoidal fit to the variation, during solar cycles 21, 22 and 23, of the UV solar flux in given spectral subintervals is performed. For more details on how this

[3]F10.7 is the full-disc solar emission at the 10.7 cm wavelength, expressed in units of 10^{-22} W m^{-2} hz^{-1}. It is often used as an indicator ("proxy index") of the general level of solar activity. However, there are some indications that this index is not a good proxy for the UV region of the spectra (Lean, 1991). A plot displaying the time variation of this index during the last solar cycles can be seen in fig. 4 of Lean *et al.*, 2001.

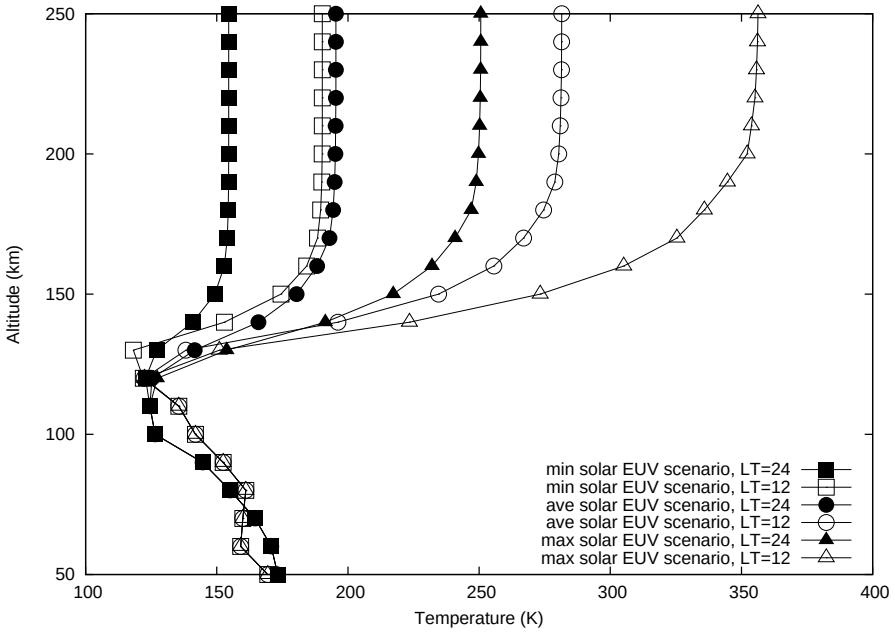

Figure 4: Example of the impact of EUV input on atmospheric temperatures. The displayed temperature profiles are those obtained at longitude 160° East, latitude 30° South, during Southern Hemisphere Spring (Ls=225°), at midday (i.e. at local time LT=12 hours, open symbols) and midnight (local time LT=24 hours, filled symbols), for minimum, average and maximum solar EUV scenarios (and fixed, MY24 dust scenario).

solar variability is included in the GCM, see González-Galindo *et al.* (2005).

4.2 The Dust Scenarios

This section outlines the dust distribution scenarios used for the GCM integrations which make up the Mars Climate Database. For the detailed rationale behind these choices (except for the MY24 scenario developed more recently) summaries of observational evidence and more references see Forget *et al.* (1999) and Lewis *et al.* (1999).

4.2.1 Dust Vertical Distribution Analytical Function

For all the scenarios, the vertical distribution of dust was calculated according to the formula,

$$\frac{Q}{Q_0} = \exp\left(0.007\left(1 - \max\left[\left(\frac{P_0}{P}\right)^{(70\mathrm{km}/z_{\max})}, 1\right]\right)\right) \tag{3}$$

with P the pressure, P_0 a standard pressure (700Pa), Q and Q_0 the dust mixing ratio at the pressure levels P and P_0, and $z_{\max}$ the altitude of the top of the dust layer (where the dust mixing ratio is one thousandth of its value at P_0). This formula gives a rapid decay up to the height of the top of the dust layer and almost homogeneous dust mixing in the lower regions of the atmosphere. The function is illustrated for several different values of $z_{\max}$ in Figure 5.

In fact, Equation 3 was developed from a slightly simpler form in common use for Mars modelling, namely,

$$\frac{Q}{Q_0} = \exp\left(\nu\left(1 - \left(\frac{P_0}{P}\right)\right)\right) \tag{4}$$

where ν is now a parameter which determines the dust cut-off. This function is illustrated in Figure 6. Equation 4 matches Equation 3 when $z_{\max} = 70$km and $\nu = 0.007$, which were

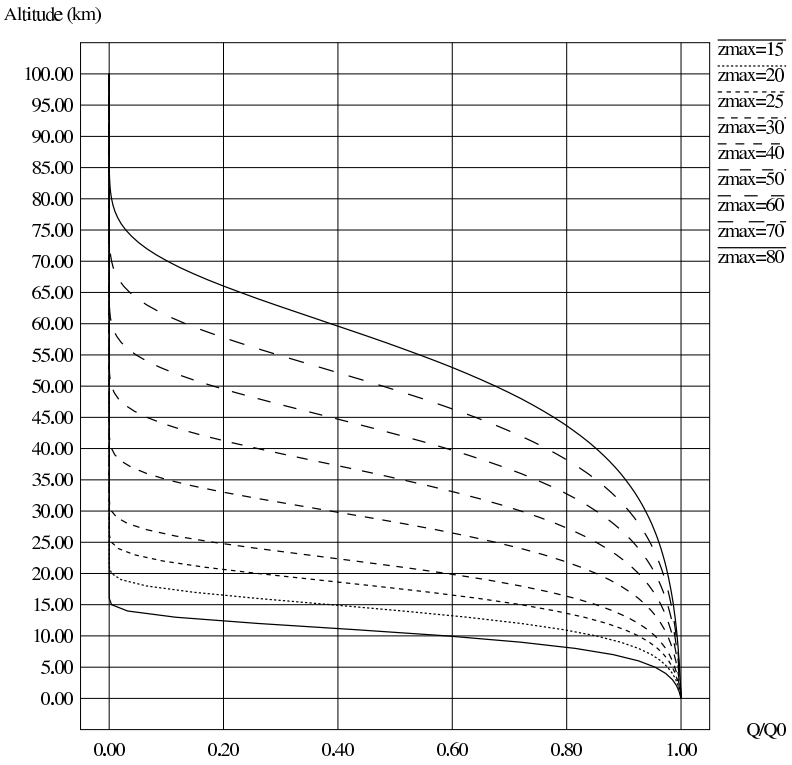

Figure 5: The variation of dust mixing ratio with height for different values of $z_{\max}$ according to the formula (Equation 3) used to compile the Mars Climate Database.

roughly the conditions under which Equation 4 was derived to model the distribution of dust at the time of the IRIS observations from Mariner 9. The reason for modifying the formula to the form in Equation 3 was that it gives much more desirable properties in terms of the total dust contained below the cut-off threshold (with a broader region of homogeneity) and the vertical gradient of the dust is not so steep near the surface, especially when the dust is mostly low in the atmosphere, compare Figure 5 with Figure 6 when $z_{\max} = 20$km and $\nu = 1.0$. While having these desirable properties the function still matches the limited available observations when the dust is high in the atmosphere.

The dust opacity of a layer l, $tau(l)$, is a function of the vertical distribution of dust in the layer $Q(l)$, the layer's pressure $P(l)$ and pressure difference $\delta P(l)$ across the layer:

$$\tau(l) = \tau_{P_0} \frac{\delta P(l)}{P_0} \frac{Q(l)}{Q_0} \tag{5}$$

where τ_{P_0} is the dust opacity at reference pressure P_0.

The total dust opacity τ of a column is then simply the sum of all the vertical layers' opacities:

$$\tau = \sum_{l=1}^{50} \tau(l) \tag{6}$$

4.2.2 Dust Distribution in Dust Scenarios

Global Circulation Model integrations were carried out using four kinds of dust scenarios:

- The **"Mars Year 24" (MY24)** scenario, designed to mimic Mars as observed by Mars Global Surveyor from 1999 to June 2001[4], a martian year thought to be repre-

[4]This corresponds to the 24th martian year according to the calendar proposed by R. Todd Clancy (Clancy et al., *Journal of Geophys. Res* 105, p 9553, 2000) which starts on April 11, 1955 (Ls=0°).

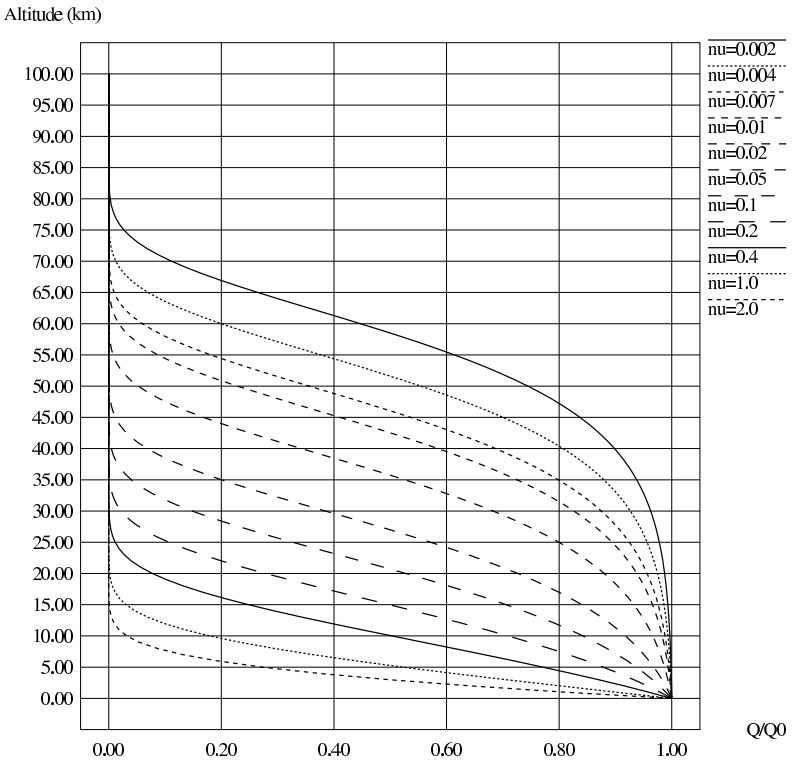

Figure 6: The variation of dust mixing ratio with height according to a formula (Equation 4) previously used in many Mars GCMs, with the ν parameter adjusted to give dust cut-offs at different heights. This function matches that in Figure 5 when $z_{\max} = 70$km and $\nu = 0.007$.

sentative of one without a global dust storm. The dust fields were derived from MGS TES observations using data assimilation technique. The MY24 scenario is provided with 3 solar EUV conditions: solar minnimum, solar average or solar maximum.

- The **cold scenario** corresponds to an extremely clear atmosphere ("Low dust scenario"; dust opacity $\tau = 0.1$), topped with a solar minimum thermosphere.
- The **warm scenario** corresponds to "dusty atmosphere for the season" scenario (but not a global dust storm), topped with a solar maximum thermosphere.
- The **dust storm scenario** represents Mars during a global dust storm (dust opacity set to $\tau = 4$). Only available when such storms are likely to happen, during northern fall and winter ($Ls \in [180, 360]$), but with 3 solar EUV conditions: solar minnimum, solar average or solar maximum.

The details of the dust distribution for these dust scenarios follows.

The Mars Year 24 Scenario

This scenario is the new, standard baseline scenario which mimics Mars as observed by Mars Global Surveyor during Mars Years 24-25, a martian year representative of one without a global dust storm. The longitude-latitude-time distribution of dust prescribed for the GCM runs used to build the MY24 Scenario is derived from the assimilation of MGS TES total optical depth observations (see Montabone *et al.*, 2006 and Lewis *et al.*, 2007). The temporal evolution of optical depth τ over the year thus obtained is displayed in Figure 7.

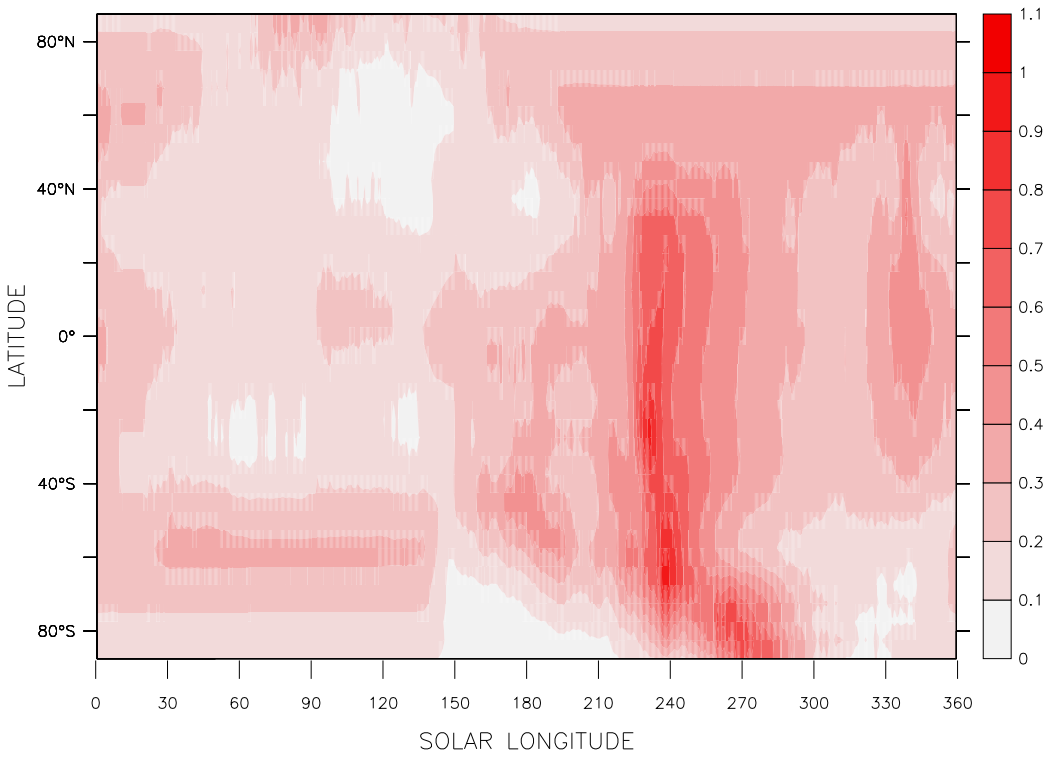

Figure 7: Zonal average of optical depth τ at reference pressure of 700 Pa for the MY24 dust scenario.

For this scenario, the cut-off of the dust in the vertical, $z_{\max}$ (in km), is a function of both latitude ϕ and solar longitude Ls:

$$z_{\max}(L_s, \phi) = 60 + 18f - (32 + 18f)\sin(\phi)^4 - 8f\sin(\phi)^5 \tag{7}$$

where $f = \sin(L_s - 160°)$. The spatial and temporal evolutions of $z_{\max}$ are represented in Figure 8.

The Warm Scenario

This dust scenario (called the Viking scenario in early versions of the MCD) provides an "upper limit" scenario, outside global dust storms, for the dust content in the Martian atmosphere. The total dust optical depth for this case varies as a function of time to fit the Viking Lander observations with peaks representing dust storms removed,

$$\tau(L_S) = 0.7 + 0.3\cos(L_S + 80°) \tag{8}$$

where τ is the optical depth and L_S the Solar longitude of Mars. The optical depth is uniform in the horizontal for the warm run. However, the cut-off of the dust in the vertical varies as a function of both time and latitude,

$$z_{\max}(L_S, \phi) = \left(60 + 18\sin(L_S - 158°) - 22\sin^2\phi\right)\text{km} \tag{9}$$

where ϕ is the latitude. $z_{\max}$ varies between 78 km at the equator during the dusty seasons and 20 km at the pole during the clear seasons. The spatial and temporal evolutions of $z_{\max}$ are represented in Figure 9.

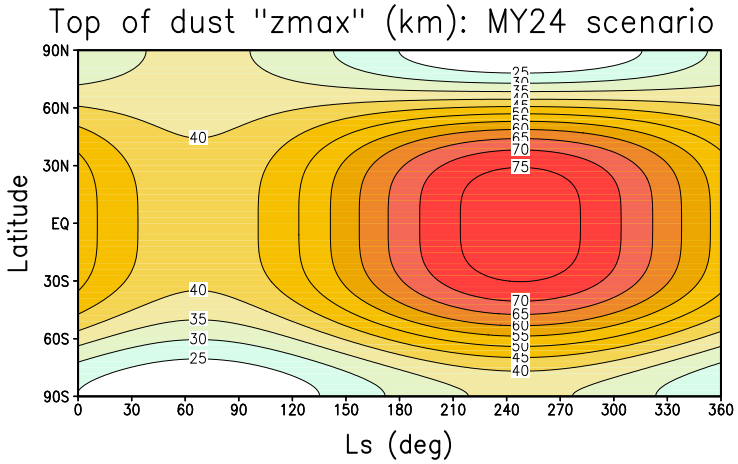

Figure 8: Cut-off altitude z_{max} (see Eq. 7) of the dust distribution as a function of solar longitude L_s and latitude for the MY24 scenario. Note that the dust storm scenario also uses this cut-off altitude.

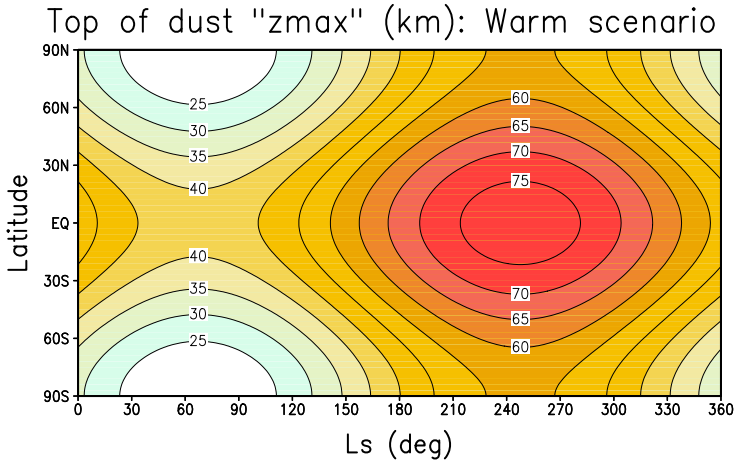

Figure 9: Cut-off altitude z_{max} of the dust distribution as a function of solar longitude L_s and latitude for the warm (Viking) scenario (see Eq. 9).

The Cold Scenario

The cold scenario corresponds to an extremely clear atmosphere, with the dust distribution set to be invariant in latitude, longitude and time, with an optical depth of $\tau = 0.1$ (at 700 Pa) and a cut-off at $z_{max} = 30$ km altitude.

The Dust Storm Scenario

For dust storm scenario runs, the dust opacity is set to $\tau = 4$ (at 700 Pa), i.e. representative of a very dusty atmosphere. Output from these (multiannual) runs are only given when such storms are most likely to happen, from northern hemisphere fall to winter ($L_S \in [180, 360]$).

For this scenario, the cut-off of the dust in the vertical, $z_{\max}$ (in km), is taken to be latitude and time dependent, just as in the MY24 scenario (see Eq. 7).

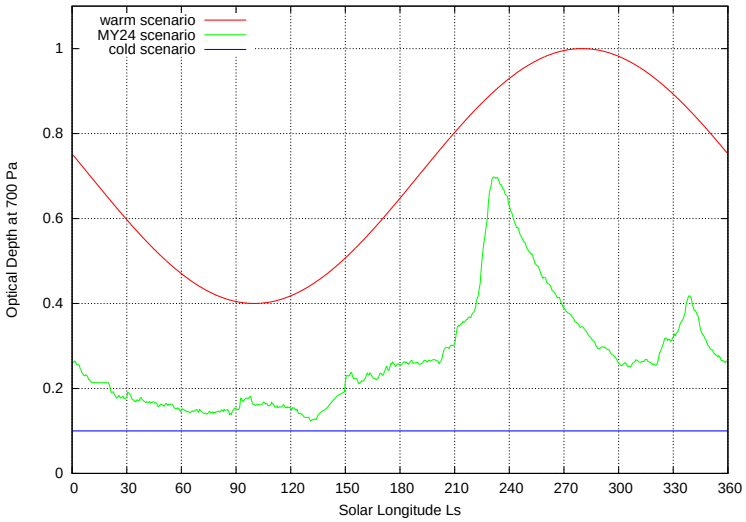

Figure 10: Visible dust opacity τ (at 700 Pa) evolution with solar longitude Ls for the warm, MY24 and cold scenarios. Values given for the MY24 scenario are mid-latitudinally averaged (i.e. mean value computed over the $[45S : 45N]$ latitude band).

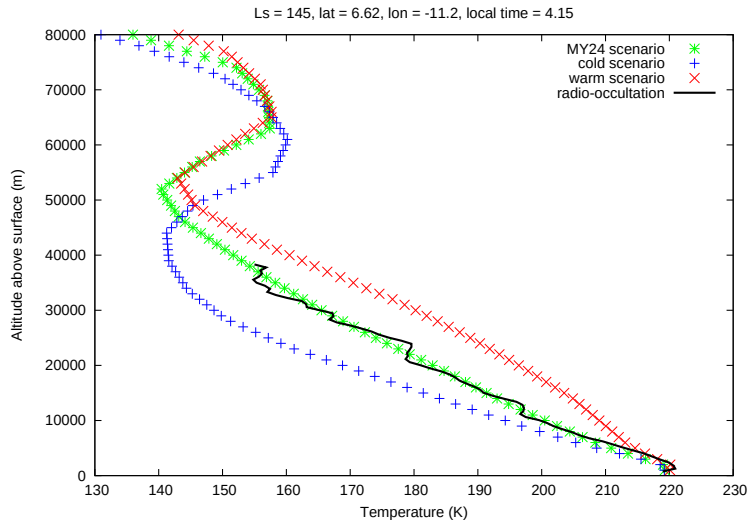

Figure 11: A typical temperature profile obtained by MGS radio-occultation in May 1999, compared to temperature profiles predicted by the MCD at the same time and location. Profiles obtained using the MY24 scenario are usually close to the MGS observations, whereas thoses obtained using the warm (i.e. dusty) and cold (i.e. low dust) scenarios are typically respectively warmer and colder.

Illustrative Examples of Dust Scenario Scopes

The various scenarios are provided to bracket the possible global (mean) atmospheric conditions on Mars. The atmospheric dust loading that is taken into account for the **MY24**, **warm** and **cold** scenarios is given in Figure 10, which summarizes and illustrates the range and variations of dust opacity included in each case.

As can be expected, atmospheric temperatures predicted by the database baseline **MY24** scenario generally compare well with observations, whereas the **warm** and **cold** scenarios respectively yield warmer and colder temperature profiles in the lower atmosphere, as illustrated in Figure 11.

5 Technical description of Methods Used to Retrieve Data from the MCD

5.1 Temporal Interpolations

Once the time of year and of day at which data is requested is known (see Appendix A for details on how these can be computed for a given Julian date), linear interpolation between datasets of encompassing months along with linear interpolation between encompassing stored martian hours are used to evalute data on the GCM grid.

5.2 Spatial Interpolations

5.2.1 Horizontal Interpolation

To compute the values of variables at a given location (which is not on the GCM grid), one needs to first build a virtual column of data along what would have been GCM levels. This profile is obtained by horizontal interpolation of encompassing grid values. To be specific, values of variables are obtained from encompassing grid values using bilinear interpolation, exept for density ρ (and similar bi-products such as associated RMS or surface pressure), which is obtained using bilinear interpolation of $\log(\rho)$.

5.2.2 Vertical Interpolation

In order to compute the value of meteorological variables at a given height (or pressure), one must first identify the altitudes (and pressure) of the vertical levels of the profile. This is done by integrating the hydrostatic equation over the column:

$$\frac{\partial P}{\partial z} = -g.\rho = -g.\frac{P}{R.T} \tag{10}$$

from which the relation between an increment in altitude δz and average (over δz), gas constant R_m, atmospheric temperature $T_m = \delta T / \log(\delta T)$, and log pressure increment $\delta \log P$ can be derived:

$$\delta z = -\frac{R_m}{g_m}.T_m.\,\delta \log P \tag{11}$$

This relation can be used to compute the altitudes of all the levels of a profile for which pressure $P(l)$ (or equivalently sigma levels $\sigma(l) = P(l)/P_S$, where P_S is surface pressure), atmospheric temperature $T(l)$ as well as gas constant $R(l)$ at all l levels are known. Moreover, as the database extends to high altitudes, it must also taken into account that gravity g varies as the inverse square of the distance to the center of the planet, i.e. that gravity at altitude z can be approximated as $g(z) = g_0.a_0^2/(a_0+z)^2$, where z is the altitude above the areoid a_0, and $g_0 = 3.7257964 m/s^2$ is the gravity at $a_0 = 3.39610^6 m$.

The altitude of the first atmospheric layer is thus obtained using:

- Gravity $g(l=1)$ is approximated to be that at the surface (of known orography, i.e. altitude above areoid, h):

$$g(l=1) = g_0.a_0^2/(a_0+h)^2$$

- The altitude of the first layer is then simply

$$z(l=1) = -[R(l=1)/g(l=1)].T(l=1).\log(\sigma(l=1))$$

From there, the altitudes of layers are recursively determined; i.e. for layer $l+1$:

- Approximate $g(l+1)$ using the altitude $z(l)$ of previous layer:

$$g(l+1) = g_0.a_0^2/(a_0+h+z(l))^2$$

- Compute altitude of level $l+1$:

$$z(l+1) = z(l) - [R(l+1)/g(l+1)].T(l+1).\log[\sigma(l+1)/\sigma(l)]$$

Once the altitudes $z(l)$ of layers are known, then the value of a variable X at a given altitude above the surface z_s may be obtained from linear interpolation of values at encompassing grid points. For variables which are, to first order, exponentially distributed in altitude (e.g. pressure, density and associated variables) then the interpolation must naturally be performed on the logarithm of these values.

5.2.3 Specific Treatments of Vertical Interpolation

Interpolation, as explained above, is feasible when the altitude (or pressure) at which the value of a variable is sought falls in the range of the MCD grid. In the more extreme cases, either above the topmost atmospheric layer or below the lowest one, different approaches must be used. These are detailed here.

Above the MCD Topmost Layer

If above the MCD topmost layer $l = L$, then pressure $P(z_s)$ at altitude z_s above the surface is extrapolated assuming a hydrostatic vertical profile, i.e.:

$$P(z_s) = P(L)\exp\left[(z(L)-z_s).g(z_s)/(R(L).T(L))\right]$$

where $P(L)$, $R(L)$ and $T(L)$ are the pressure, gas constant and temperature at layer L, $z(L)$ its altitude and $g(z_s)$ is gravity at altitude z_s.
Density ρ, as well as the RMS of these two variables, are treated similarly.

All other variables are not extrapolated and are assumed to remain constant above the topmost layer.

Below the Lowest MCD Layer

When below the lowest MCD layer $l = 1$ (which typically lies at 5 m above the surface, see table in Section 3.4.2), then pressure $P(z_s)$ at altitude z_s above the surface is computed using a hydrostatic vertical profile, i.e.:

$$P(z_s) = P(1)\exp\left[(z(1)-z_s).g(z_s)/(R(1).T(1))\right]$$

where $P(1)$, $R(1)$ and $T(1)$ are the pressure, gas constant and temperature at the first,layer, $z(1)$ its altitude and $g(z_s)$ is gravity at altitude z_s. This formulation enables recovery of the value of surface pressure Ps when $z_s = 0$.
Density ρ, as well as the RMS of these two variables, are treated similarly.

Other variables (except horizontal winds and atmospheric temperature) are not extrapolated and are taken to be constant from the middle of the first atmospheric level down to the surface.

Near Surface Atmospheric Temperature

Since the value of surface temperature Ts is part of the data provided in the MCD, atmospheric temperature at an altitude z_s between the surface and the middle of the first atmospheric layer $l = 1$ is computed using linear interpolation:

$$T(z_s) = Ts + (z_s/z(1)).(T(1) - Ts)$$

where $T(1)$ is the temperature of the first layer and $z(1)$ its altitude.

Near Surface Horizontal Winds

The Global Circulation Model which is used to compile the MCD includes parametrizations to account for various sub-grid phenomena, which includes (among many other items) the fact that near the surface, a logarithmic boundary layer develops. This distribution of horizontal winds is thus also taken into account when values of horizontal winds are sought between z_0, the roughness length (currently set to 0.01 m in the GCM) and the middle of the first atmospheric layer. In such cases, the (meridional or zonal) wind $u(z_s)$ at altitude z_s above the surface is given by:

$$u(z_s) = u(1)\frac{\log(z_s/z_0)}{\log(z(1)/z_0)}$$

where $u(1)$ is the (meridional or zonal) wind of the first layer and $z(1)$ its altitude.

The values of the horizontal winds are set to zero below the roughness length z_0.

6 Variability Models in the MCD

6.1 Day-to-Day RMS of Variables

The MCD provides the day-to-day variability of variables computed from the outputs of the Global Circulation Model (GCM). This day-to-day RMS of variable X is computed over each month as:

$$RMS(X) = \sqrt{\frac{1}{N}\sum_{1}^{N}\left(< X >_{1\text{ sol}} - < X >_{10\text{ sols}}\right)^2} \tag{12}$$

where N is the number of samples from the time-series output of variable X over the month and $< X >_{1\text{ sol}}$ and $< X >_{10\text{ sol}}$ respectively denote running averaged values of X over a sol and 10 sols.

The RMS thus obtained represents the variability of a variable from one day to the next, at a given time of the day, regardless of the general drift over the month (removed by taking into account the deviation of diurnal values to 10-day averages, i.e. long term trends, in the computation of the RMS). The connection between day-to-day variability, 1-day and 10-day averages is illustrated in Figure 12.

It is important to note that the RMS values obtained from the GCM outputs are computed on the GCM grid and that since the vertical coordinate is essentially (see Section 3.4.2) a pressure coordinate, the obtained RMS values are evaluated at constant pressure.

Apart from this pressure-wise RMS, the MCD now also provides altitude-wise RMS, which is computed in the same way, but on time series of GCM outputs which have been interpolated on a fixed altitude vertical coordinate grid. For some variables, which are dependent on pressure, e.g. density, the difference between pressure-wise and altitude-wise RMS can be quite significant.

6.2 The Large-Scale Variability Model

In the MCD, data are stored in 12 monthly bins and at 12 local times of day within each season. Although this captures the main seasonal and diurnal components of variability, any intra-month or day-to-day (synoptic) variations are averaged out. Thus there is a need to simulate this variability, especially if the user wishes to produce an ensemble of realizations of a variable at a particular seasonal date and local time of day which covers a realistic range of variability.

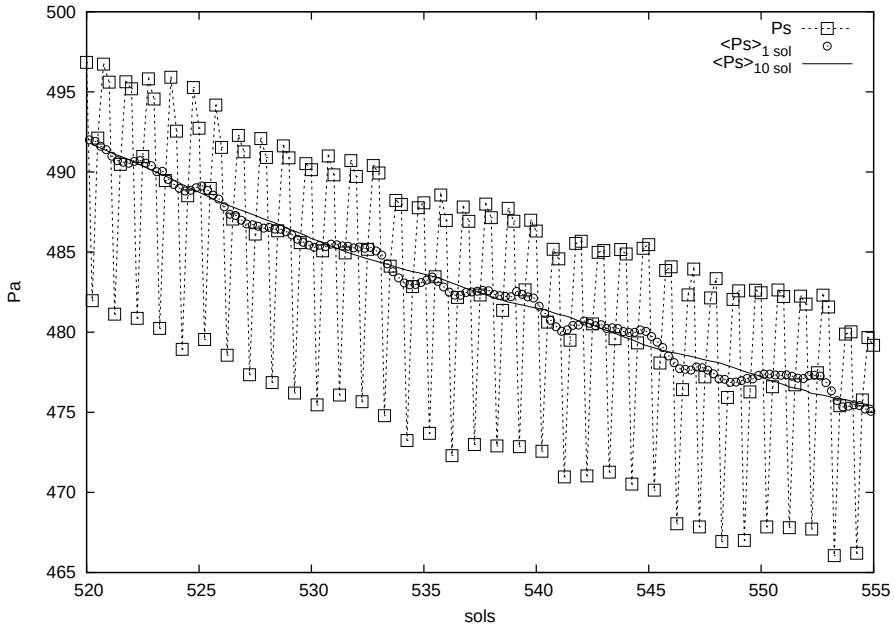

Figure 12: Time-series (4 samples per sol) of surface pressure (squares) obtained at a grid point (located at longitude 135 degress east and latitude 30 degrees south) of the Global Circulation Model run corresponding to the 10th month of the MY24 dust scenario. Also shown on the figure are the 1-day (circles) and 10-day (solid line) averages of the time series from which the day-to-day RMS of surface pressure is computed (see text).

In version 1.0 of the MCD large-scale variability in a vertical profile of a meteorological variable, $D(z)$, was modelled by adding a series of functions to a mean vertical profile, $\overline{D}(z)$,

$$D(z) \ = \overline{D}(z) \ + \ \sum_{i=1}^{I} \ p_i \mathbf{e}_i(z) \tag{13}$$

where the functions $\mathbf{e}_i(z)$ are eigenvectors of the covariance matrix of all the pre-averaged profiles generated by the GCM and p_i are the amplitudes of the functions. The eigenvectors, $\mathbf{e}_i$, are often called Empirical Orthogonal Functions (EOFs) and the p_i are referred to as the Principal Components (PCs) (see, e.g. North, 1984; Mo and Ghil, 1987). The set $\{\mathbf{e}_i\}$ form an optimal linear basis such that the variance capture is high even when the truncation limit is low.

6.2.1 Horizontal Correlations

In version 1.0 only correlations in altitude between variables were considered when calculating the covariance matrix. However, in order to retain cross-correlations between different variables (zonal wind, meridional wind, temperature, surface pressure and density) all were normalized and combined together to form a set of multivariate functions. Different sets of EOFs were computed for each of the 12 seasons on a low resolution grid (20° longitude $\times$ 20° latitude) and the series (13) was truncated at $I = 6$ at each location to reduce the demands on data storage. Even so, typically $80 - 90\%$ of the variance was retained in the version 1.0 variability model at this level of truncation.

In order to improve the model it is desirable to extend the spatial dimension to include correlations between variables in both the horizontal and the vertical. Ultimately it is desirable to include all the longitude, latitude and vertical grid-points in the analysis. A technical point, however, must be noted here. In computing the EOFs, the eigenvalues

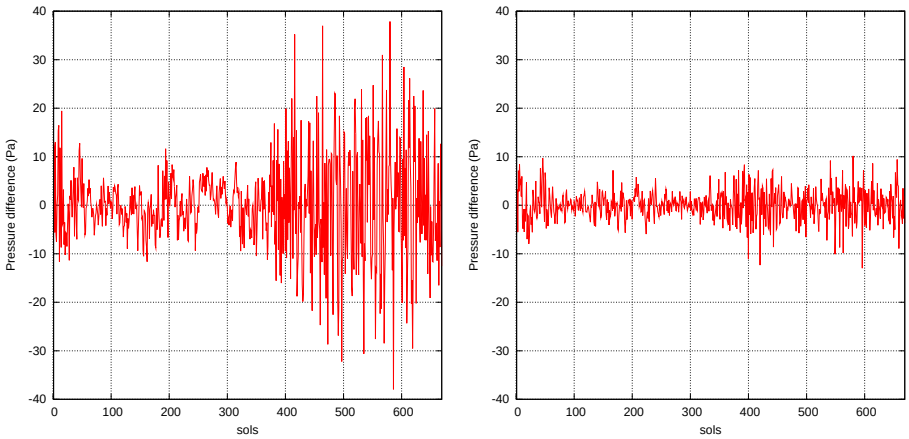

Figure 13: Illustrative example of data reconstruction quality with number of EOFs used for the reconstruction: Are displayed the 'errors' (i.e. differences between true value and reconstructed value) of surface pressure at a given location (lon=135 E and lat=52.5 N; a grid point near VL2 site) when using 72 EOFs (left plot) or 200 EOFS (right plot).

and eigenvectors of an $N \times N$ real symmetric matrix must be found. The order, N, of the matrix depends on the number of variables and on the number of spatial points. Since the number of calculations needed to perform the eigenvector problem increases as N^3 there is a limit on the value of N that can be handled practically. The estimated CPU time and storage requirements for calculating the eigenvectors of the full problem (even on a low resolution $16 \times 12 \times 50$ lon $\times$ lat $\times$ height grid with three three-dimensional -horizontal wind components and atmospheric temperature- and one two-dimensional -surface pressure- variables, for which $N = 16 \times 12 \times (3 \times 50 + 1) = 28992$) is prohibitive.

We make the choice, therefore, to calculate EOFs in the two-dimensional, height-longitude plane which gives a manageable set of eigenvector problems. There is some physical basis for this choice, in that much of the variability the model must account for is in the form of baroclinic waves which, in general, propagate West to East along lines of latitude.

6.2.2 Statistical Stability and PC Modelling

In version 1.0 of the MCD we calculated separate sets of the variability EOFs for each of the 12 months. However, due to the relatively small number of days in each month (46–66), this can lead to poor estimation of the EOFs. Greater statistical stability can be achieved by forming the covariance matrix over the entire annual cycle, although this means that more EOFs must be retained in the series (13) in order to still capture a relatively high fraction of the variance.

Tests with the dataset corresponding to MCD version 4.3 have shown that the original series may be reconstructed with sufficient accuracy when extended to include 200 EOFs (rather than the 72 retained in previous 4.x versions of the MCD), as illustrated in figure 13 (see also Section 6.2.4).

6.2.3 Calculation of EOFs and PCs

Consider a time series of longitude-pressure vectors of zonal wind, $u(\phi, p, t)$, meridional wind, $v(\phi, p, t)$, temperature, $T(\phi, p, t)$, and surface pressure $p^*(\phi, t)$ at M discrete time points and on L spatial points. We form a time series of vectors $\mathbf{D}(t)$, where

$$\mathbf{D}(t) \;=\; (\hat{u}(\phi, p, t), \hat{v}(\phi, p, t), \hat{T}(\phi, p, t), \hat{p^*}(\phi, t)) \qquad (14)$$

and the hat $\hat{}$ denotes a removal of the series mean and normalization of variance operator,

$$\overline{u} \;=\; \frac{1}{ML}\sum_{m=1}^{M}\sum_{l=1}^{L} u_{ml} \tag{15}$$

$$\hat{u}_{ml} \;=\; \frac{u_{ml}-\overline{u}}{\sqrt{\frac{1}{ML}\sum_{m=1}^{M}\sum_{l=1}^{L}(u_{ml}-\overline{u})^2}} \tag{16}$$

where the m denotes time and the l denotes spatial point. Hence, with this normalization, the variance of the entire time series of $\mathbf{D}(t)$ is unity.

We then form the $(N \times N)$ covariance matrix, $\mathbf{C}$, such that

$$\mathbf{C} \;=\; \frac{1}{N}\mathbf{D}\mathbf{D}^T \tag{17}$$

where N = (number of horizontal points) $\times$ (3 $\times$ number of vertical points + 1), $\mathbf{D}$ is the $(N \times M)$ matrix whose rows are the vectors $\mathbf{D}(t)$ and the superscript T indicates the transpose.

The matrix $\mathbf{C}$ is real symmetric and we can find the eigenvectors and eigenvalues and order them in decreasing eigenvalue magnitude. We note that if $\mathbf{E}_i$ is the ith eigenvector then

$$|\mathbf{E}_i| \;=\; 1 \tag{18}$$

where $|\cdot|$ is the Euclidean Norm, and

$$\sum_{i=1}^{N}\lambda_i \;=\; 1 \tag{19}$$

where λ_i is the ith eigenvalue.

The ith principal component (PC) at time m, p_{mi} is defined as

$$p_{mi} \;=\; \sum_{n=1}^{N} D_{mn}E_{ni} \;=\; \mathbf{D}\cdot\mathbf{E}_i \tag{20}$$

and we note the result

$$\frac{1}{MN}\sum_{m=1}^{M}(p_{mi})^2 \;=\; \lambda_i \tag{21}$$

Each principal component has 669 values during one year (one per day). From the PCs can be calculated a 31 day running mean, ps_{mi} which can be used to reconstruct a smoothed version of the original signal, as shown in figure 14.

6.2.4 The Large Scale Perturbation Model

Using PCs and their smoothed version provides a mean to store variability: as can be infered from figure 14, the difference between reconstructions reflects, to a great extent, typical daily deviations to mean behaviour which can be used to generate realistic sets of large scale coherent perturbations.

The scheme to build large scale perturbations to add to mean variables in MCD v4.3 is thus simply to compute deviations as described above, but at a time t' which is randomly determined within a 31 sol window of current time t. The deviation obtained for time t' is then simply added to the mean values of variables at time t. Note that since it is a simple "time shift" which is used to build the perturbation, coherence between variables and over any distance is preserved as long as t' is kept fixed.

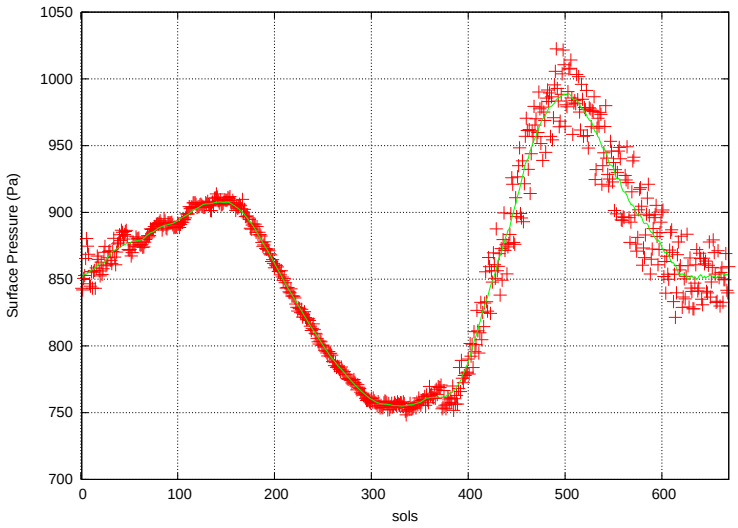

Figure 14: Example of data reconstruction using PCs (crosses) and their smoothed version (line). The displayed reconstructed values of surface pressure are for a grid point located at lon=135 E and lat=52.5 N, close to VL2 landing site.

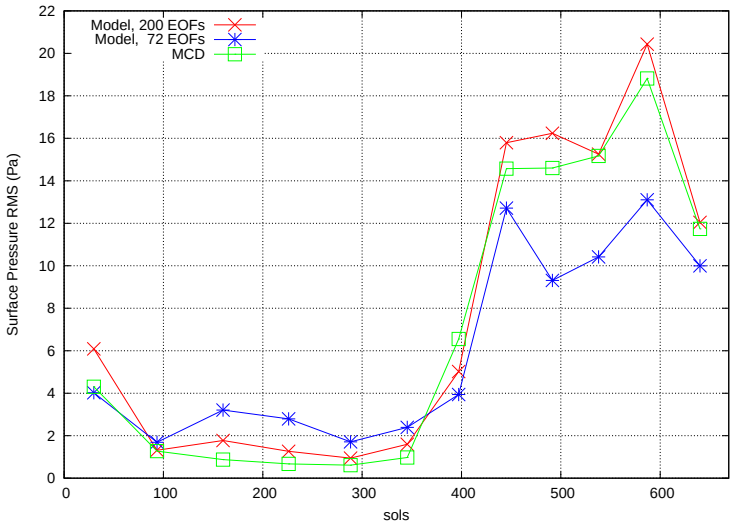

Figure 15: Example of day-to-day variability of surface pressure, computed for each of the twelve martian months, using perturbed series from the large scale perturbation model. RMS values for the original series (corresponding to data at lon=135 E and lat=52.5 N, close to VL2 landing site) are also displayed for comparison, along with the RMS values that are obtained if only 72 EOFs are used to build the perturbed series.

This approach has been validated by checking that the day-to-day variability (see section 6.1) of time series reconstructed using this model is close to that obtained for the original data, as shown in figure 15. Note that the values of RMS that are obtained when only 72 EOFs are retained to build the perturbation are also given in the figure; in this latter case the model then clearly yields a variability which is much less satisfactory.

Tests have shown that when the number of EOFs is increased, then the recomputed RMS converges towards that of the original data. However, including more EOFs would tend to increase storage requirements significantly compared to the corresponding increase in variance capture and the best compromise between variability capture and storage seems to be to retain 200 EOFs.

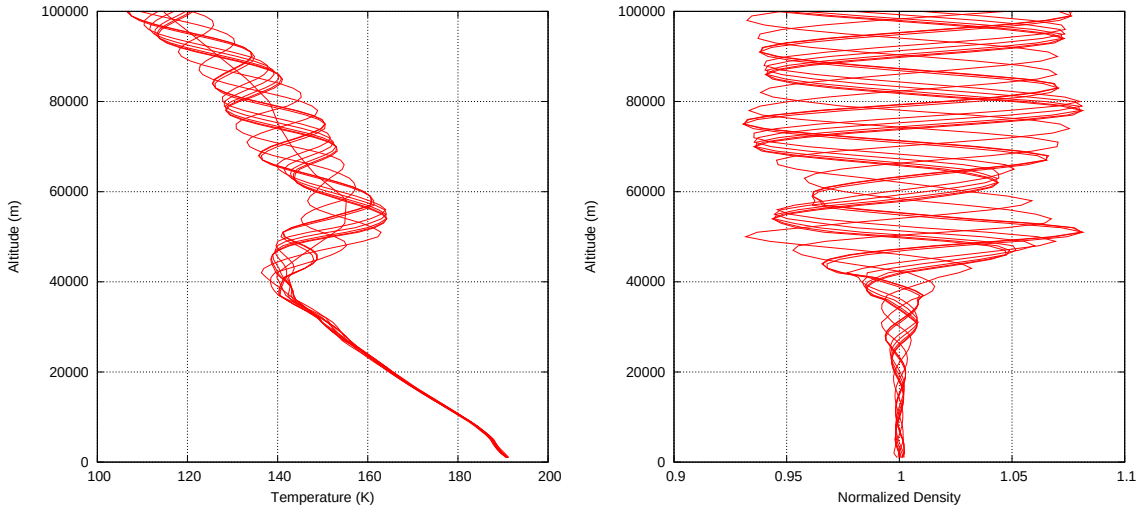

Figure 16: A series of ten perturbations, all with the same wavelength (16 km), generated by the small scale variability model added to mean profiles of temperature and density from the MCD. Left plot: Atmospheric temperatures (including unperturbed profile). Right plot: density deviations (i.e. perturbed over unperturbed density ratios). Profiles obtained at longitude 230° East, latitude 30° South, Solar Longitude Ls=73° and a local time of 10 hours.

6.3 The Small-Scale Variability Model

The small-scale variability model simulates perturbations of density, temperature and wind due to the upward propagation of small-scale gravity waves. The model is based on the parameterization scheme used in the numerical models that simulated the data in the database (see Collins *et. al*, 1997).

The surface stress exerted by a vertically-propagating, stationary gravity wave can be written

$$\tau_0 \;=\; \kappa\rho_0 N_0 |\mathbf{v_0}| \sigma_0 \tag{22}$$

where κ is a characteristic gravity wave horizontal wave number, ρ_0 is the surface density, N_0 is the surface Brunt Väisälä frequency, $\mathbf{v_0}$ is the surface vector wind and σ_0 is a measure of the orographic variance. In this case we choose the model sub-grid scale topographic variance. The surface stress can be related to the gravity wave vertical isentropic displacement, δh, by

$$\tau_0 \;=\; \kappa\rho_0 N_0 |\mathbf{v_0}| \delta h^2. \tag{23}$$

We then assume that the stress, τ, above the surface is equal to that at the surface. This leads to an expression for the wave displacement δh, at height z,

$$\delta h \;=\; \sqrt{\frac{\rho_0 N_0 |\mathbf{v_0}| \sigma_0}{\rho N |\mathbf{v}|}} \tag{24}$$

where ρ, N and $\mathbf{v}$ are the density, Brunt Väisälä frequency and wind vector at height z.

The gravity wave perturbation to a meteorological variable is calculated by considering vertical displacements of the form

$$\delta z = \delta h \sin\left(\frac{2\pi z}{\lambda} + \phi_0\right) \tag{25}$$

where λ is a characteristic vertical wavelength for the gravity wave and ϕ_0 is a randomly generated surface phase angle. Perturbations to temperature, density and wind at height z

are then found by using the value at $z+\delta z$ on the background profile, with the perturbations to temperature and density calculated on the assumption of adiabatic motion to the valid height. A value can be chosen for λ (we take $\lambda = 16$ km as a default, as it provides a reasonable comparison with the observed Viking entry temperature profiles above 50 km), in the range of 2-30 km; longer vertical wavelength should be well resolved by the model and shorter wavelengths result in negligible perturbations. An example of several small scale perturbations is shown in Figure 16.

7 High Resolution Outputs

The Mars Climate Database has been compiled from the output of a general circulation model in which the topography is very smoothed because of its low resolution. In addition, the pressure variations due to the CO_2 cycle (condensation of atmospheric CO_2 in the polar caps) that is computed by the model is only based on the simulation of the actual physical processes. The polar cap physical properties have been tuned somewhat to reproduce the observations, but no correction was added.

As of version 4.2, the access software includes a "high resolution" mode which combines high resolution (32 pixels/degree) MOLA topography and the smoothed Viking Lander 1 pressure records (used as a reference to correct the atmospheric mass) with the MCD surface pressure in order to compute surface pressure as accurately as possible. The latter is then used to reconstruct vertical pressure levels and hence, within the restrictions of the procedure, yield high resolution interpolated values of atmospheric variables.

All these post-processing procedures are detailed in the following subsections.

7.1 High Resolution Topography and Areoid

The MCD includes (and uses) topography and areoid (Mars geoid) at the database's resolution (64×49 in longitude×latitude). The need to yield higher resolution outputs has led to the development of post-processing tools which require knowledge of these two fields at a much higher resolution. This is achieved using the most up-to-date models and datasets distributed by the Mars Orbiter Laser Altimeter (MOLA) Team.

7.1.1 Mars Gravity Model

Very high resolution values of the Martian areoid can be computed using the MGM1025 spherical harmonic solution of the Mars gravity field to degree and order 80, using X band tracking data of the MGS Mars Orbiter Laser Altimeter. This model is an update of the Goddard Mars Model 2B (GMM2B) described in Lemoine *et al.* (2001) and follows the IAU2000 rotation model and cartographic frame (see Seidelmann *et al.*, 2002) recommended by the Mars Cartography Working Group.

A Fortran program to compute the radius of the geoid at given areocentric latitude and longitude, along with a file containing the MGM1025 coefficients, are kindly made available by G. Neumann from:
`http://ltpwww.gsfc.nasa.gov/tharsis/data.html`
The supplied `areoid.f` program was adapted and merged into the MCD `heights.F` collection of routines which uses the MGM1025 gravity field coefficients (file `mgm1025` in `data` directory of the MCD DVD) obtained from the same source.

7.1.2 MOLA Topography

The MOLA Precision Experiment Data Record (PEDR) are archived and distributed by the Planetary Data System (`http://pds.jpl.nasa.gov`) and include topography data binned at various resolutions (from 4 pixels per degree to 128 pixels per degree for the whole planet and up to 512 pixels per degree in the polar regions).

The 32 pixel per degree topography file (a binary file) was converted to NetCDF, yielding the 'mola32.nc' file (in the `data` directory of the MCD DVD) which is used by MCD software. The choice of this resolution as "high resolution" results from a compromise between datafile size and need for resolution (32 pixels per degree corresponds to a 1850 m resolution at the equator, where the mesh is largest): the file `mola32.nc` is already a 127 Mb file (a higher resolution 64 pixels per degree topography file would be 4 times bigger, i.e. around 520 Mb).

7.2 Deriving High Resolution Surface Pressure

High resolution surface pressure may be obtained from GCM surface pressure by using Viking Lander 1 records to correct atmospheric mass and by taking into account the change in altitude from the (coarse and smoothed) GCM topography to more realistic high resolution topography.

In practice, an estimation of the high resolution surface pressure Ps at a given location and time is given by:

$$Ps = Ps_{\rm GCM} \ \frac{< P_{\rm VL1_{OBS}} >}{< P_{\rm VL1_{GCM}} >} \ e^{-(z-z_{\rm GCM})/H} \tag{26}$$

where $Ps_{\rm GCM}$ is the pressure predicted by the GCM at the same location and time (bilinear interpolations from the MCD grid), $< P_{\rm VL1_{OBS}} >$ the VL1 surface pressure records smoothed to remove thermal tides and transient waves, taken from Hourdin *et al.* (1993), $< P_{\rm VL1_{GCM}} >$ the similarly smoothed (i.e. diurnally averaged) VL1 surface pressure predicted by the GCM (interpolated vertically and horizontally), z is the altitude of the local surface retrieved from the MOLA dataset, and $z_{\rm GCM}$ is the altitude at the location interpolated from the coarse GCM topography grid. H is the scale height used in the hydrostatic equation to vertically interpolate the pressure: $H = RT/g$ with R (m^2 s^{-2} K^{-1}) the gas constant, $g = 3.72$ m s^{-2} the acceleration of gravity, and T the atmospheric temperature extracted from the GCM at about 1 km above the surface[5]. The choice of this altitude to interpolate surface pressure on Mars is based on the theoretical considerations and tests described in Spiga *et al.* (2007).

This procedure to predict high resolution surface pressure was initially provided with Mars Climate Database version 4.1, as a distinct external tool, 'pres0'. As of version 4.2 of the MCD, the main routine 'call_mcd' can yield high resolution outputs and uses the procedure described above to derive high resolution surface pressure values. The 'pres0' tool is still provided as a standalone tool (which uses data files `VL1.ls`, the smoothed VL1 surface pressure, `mola32.nc` for the high resolution topography and file `ps_MY24.nc` which simply contains the minimal subset of data from the MCD required for the algorithm).

An example of the impact of the high resolution scheme is given in Figure 17 where are plotted the surface pressure, at GCM resolution, at VL1 site along with the pressure (at the same elevation) that is obtained (see next section) from the high resolution surface pressure derived using the scheme described above. Note that due to the "total atmospheric mass correction" term, the $< P_{\rm VL1_{OBS}} > / < P_{\rm VL1_{GCM}} >$ ratio in Eq. 26, the difference between GCM resolution and high resolution pressures at a fixed location varies non-monotonically with solar longitude.

7.3 Computing High Resolution Values of Atmospheric Variables

7.3.1 Interpolation of Atmospheric Temperature

The MCD contains the atmospheric temperatures obtained from the corresponding GCM runs, on the same grid (as described in Section 3.4), and thus at given pressure $P(l)$ for a given location and layer l (computed from surface pressure $Ps_{\rm GCM}$ interpolated from the 3.75° latitude by 5.625° longitude 64×49 MCD grid, using Equation 1 as shown in Section 3.4.2). If, however, the surface pressure should in fact be $Ps_{\rm HR}$, as given by Equation 26, then a legitimate question is then: How should the atmospheric temperature profile $T(l)$ above $Ps_{\rm HR}$ be interpolated?

To better understand this issue, i.e. the behavior of atmospheric temperature field over topography at higher resolutions, high resolution simulations (176×132 at LMD and up to

[5]Technically, the temperature that is used is that of the 7th atmospheric layer, which is located at about 1 km above the surface (see Section 3.4.2).

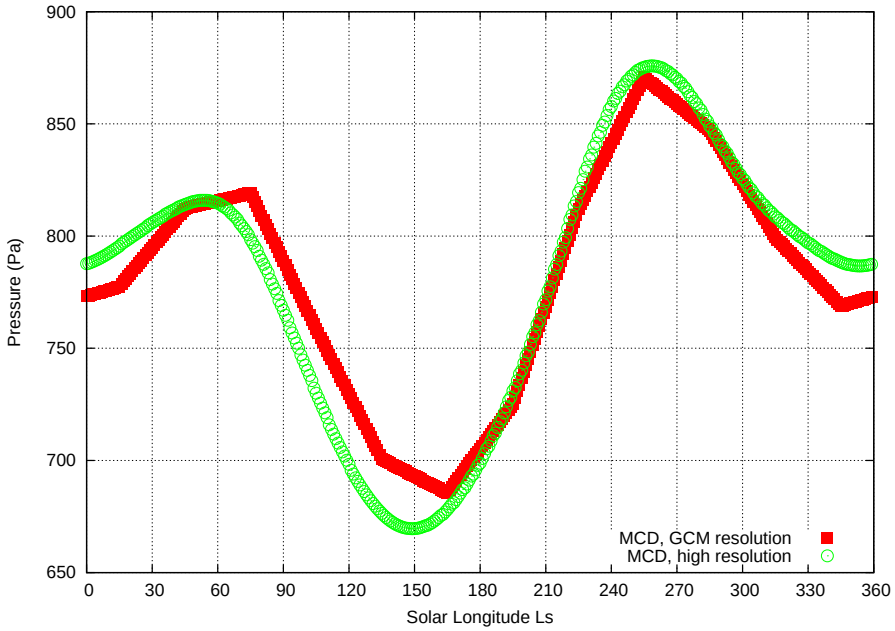

Figure 17: Illustrative example of the effect of the high resolution mode: Pressure at VL1 location (longitude $-47.949619°$ east and latitude $22.269628°$ north) and at altitude -3421.1113 m above areoid (which corresponds to the surface at GCM resolution; at high resolution the surface lies at -3637.1396 m above areoid).

512×256 at The Open University) were performed and their output compared to the lower (64×49) resolution ones.

These simulations show that temperature behaves as follows :

1. When topography -and thus surface pressure- varies locally, surface temperature is not affected (it is in radiative equilibrium; only the variation of dust opacity affects the surface temperature, but the impact should be small compared to the variations of albedo, thermal inertia, and slope).

2. To first order, temperature near the surface (first few kilometres) is controlled by the distance from the surface. Above, it is controlled by the pressure level, somewhat independenlly from the kilometre scale topography.

3. To second order, the near surface air temperature is colder in high altitude regions that in the neighbouring plains, as a result of adiabatic cooling.

4. In local depressions (crater, canyon, etc..), the opposite effect is observed (near surface air warming) but it is less significant.

These facts are taken into account to build the rules to use to interpolate temperature in "high resolution" mode: The MCD temperature profile $T(l)$ is not changed, but the corresponding pressure levels $P(l)$ are. Doing so moreover enables the use of the same database access software as with the "low resolution", except for the adjustment of pressure levels.

After a bit of tuning and applying rules 1 to 4 above, it has been found that the new "high resolution" pressure levels $P_{\rm HR}(l)$ can be built using a function designed to ensure a smooth transition from the near-surface conditions to the free atmosphere (high altitude) environment:

$$P_{\rm HR}(l) = P_{\rm GCM}(l)\ [f(l) + (1 - f(l))\ 0.5\ (1 + \tanh(6\ (-10\ \ln(\frac{P_{\rm GCM}(l)}{Ps_{\rm GCM}}) - z)/z))] \qquad (27)$$

where $P_{\rm GCM}(l)$ is the original pressure level in the database. z roughly corresponds to the altitude above the surface (in the GCM smoothed topography) where $P_{\rm HR}$ will become equal to $P_{\rm GCM}$. It varies depending on the altitude difference (derived from pressure) between the high and low resolution grid Δz (km) :

$$\Delta z = -10 \ln\left(\frac{Ps_{\rm HR}}{Ps_{\rm GCM}}\right) \tag{28}$$

And z is set to:

$$\begin{aligned} z &= \Delta z + 3 \text{ if } \Delta z > 0 \text{ (local mountain)} \\ z &= 3 \text{ if } \Delta z < 0 \text{ (local depression)} \end{aligned}$$

$f(l)$ is a variable parameter which is equal to 1 at high altitude (then $P_{\rm HR}(l) = P_{\rm GCM}(l)$). At low altitude, it is designed to ensure that the first levels will be a the same distance from the surface in both low and high resolution (then $P_{\rm HR}/Ps_{\rm HR} = P_{\rm GCM}/Ps_{\rm GCM}$ except when there is a local high topography structure (HR surface more than 1 km above the GCM surface). In such conditions the model levels are compressed closer to the surface, to mimic the observed behaviour in high resolution GCM simulations. Conversely the model levels are expanded when there is a topographic low. (HR surface more than 1 km below the GCM surface). In practice $f(l)$ is computed as:

$$f(l) = \frac{Ps_{\rm HR}}{Ps_{\rm GCM}} \left(\frac{P_{\rm GCM}(l)}{Ps_{\rm GCM}}\right)^x \tag{29}$$

where x is the parameter which control the compression of the extension of the layers near the surface (no effect when $x = 0$, compression if $x < 0$, extension if $x > 0$.
The value of x is derived from that of Δz :

$$\begin{aligned} x = &\quad 0 && \text{if } -1 < \Delta z < 1 \\ x = &\quad -0.12\ (|\Delta z| - 1) && \text{if } \Delta z > 1 \\ x = &\quad +0.12\ (|\Delta z| - 1) && \text{if } \Delta z < 1 \\ x = &\quad 0.8 && \text{if formulas above yield } x > 0.8 \\ x = &\quad -0.8 && \text{if formulas above yield } x < 0.8 \end{aligned}$$

Figures 18 and 19 display examples of the temperature fields produced by the "high resolution" MCD V4.2 compared to the "low resolution" version and true high resolution (176×132) GCM output.

7.3.2 Interpolation of Density

In the low resolution version of the database, the density ρ (kg m^{-3}) at altitude z (m) is interpolated in the vertical by using a weighted interpolation between the density at the level above (ρ_{l+1}) and the density at the level below (ρ_l). In practice the linear interpolation is performed on the logarithm of the density (as mentionned in Section 5.2.2).

Density is proportional to pressure and thus, in the "high resolution" mode, it must be re-computed by taking into account the change in pressure (computed using Equation 27). The algorithm for vertical interpolation that is used for "low resolution" density is used to compute "high resolution" density, but using $\rho_{l+1}P_{\rm HR}(l+1)/P_{\rm GCM}(l+1)$ and $\rho_l P_{\rm HR}(l)/P_{\rm GCM}(l)$ instead of ρ_{l+1} and ρ_l

A similar treatment is applied to the RMS of density, corresponding perturbations, etc...

7.3.3 Modification of Other Variables

Most other atmospheric variables X (winds, turbulent kinetic energy, gases and ice mixing ratio) are treated like temperature: the values of the profile $X(l)$ are kept, and only the pressure of the levels $P(l)$ are recomputed to account for the "high resolution" post-processing.

The water vapor column and dust optical depth τ are scaled to the high resolution surface pressure (e.g. $\tau_{\rm HR} = \tau_{\rm GCM} Ps_{\rm HR}/Ps_{\rm GCM}$). However, we do not modify the water ice column, because in most case ice areosols form well above the surface and should not be too sensitive to the kilometer scale topography.

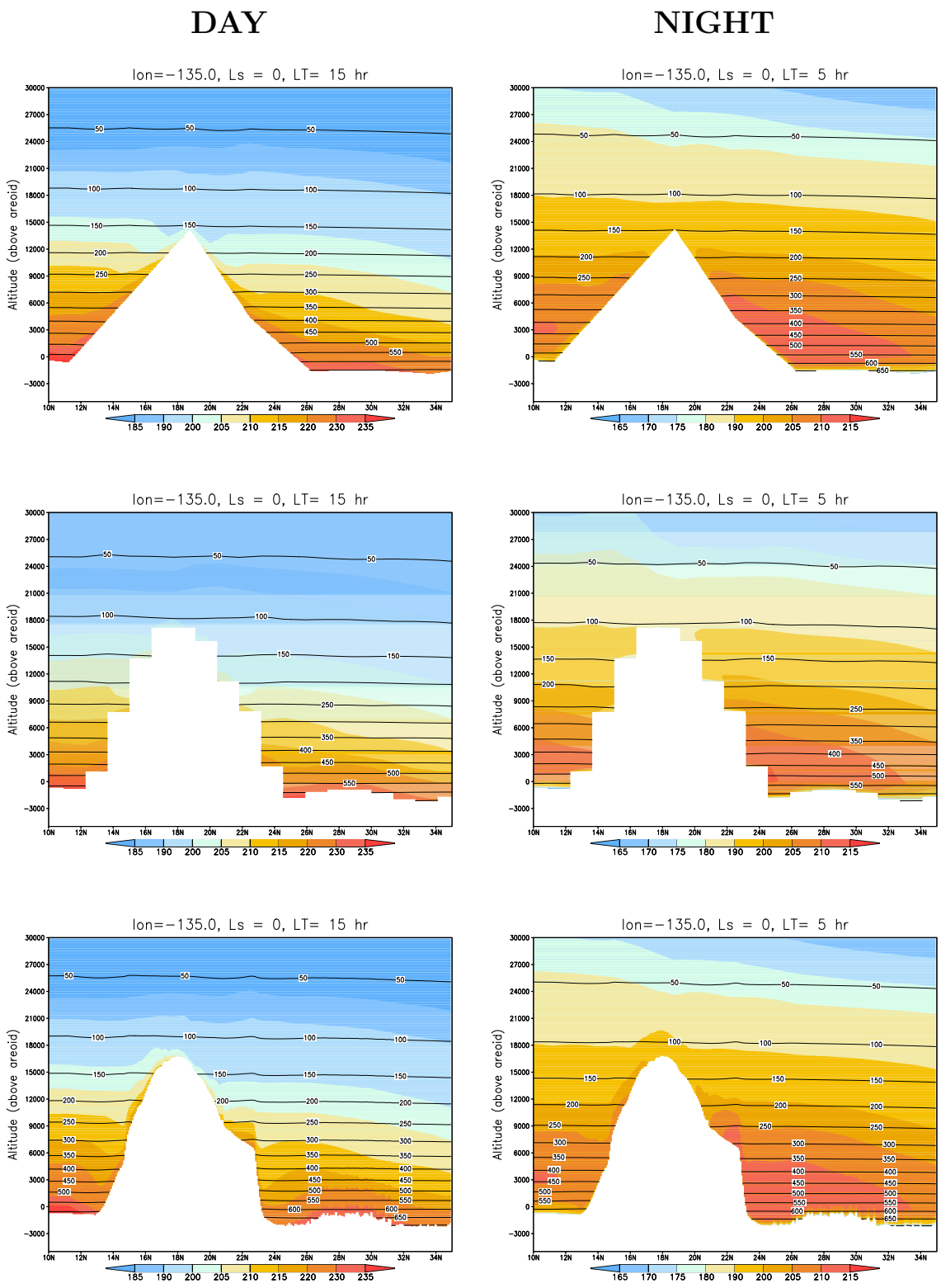

Figure 18: Cross-section of temperature fields (colored) and pressure level (black contour) near Olympus Mons from MCD V4.2 at GCM resolution (top row), from a high resolution 176×132 GCM run (middle row), and from the high resolution output of MCD v4.2 (bottom row). Note that there is an order of magnitude between horizontal and vertical scales in these plots; what appear as sharp gradients in the horizontal direction are in fact quite smooth when displayed using more commensurate axes.

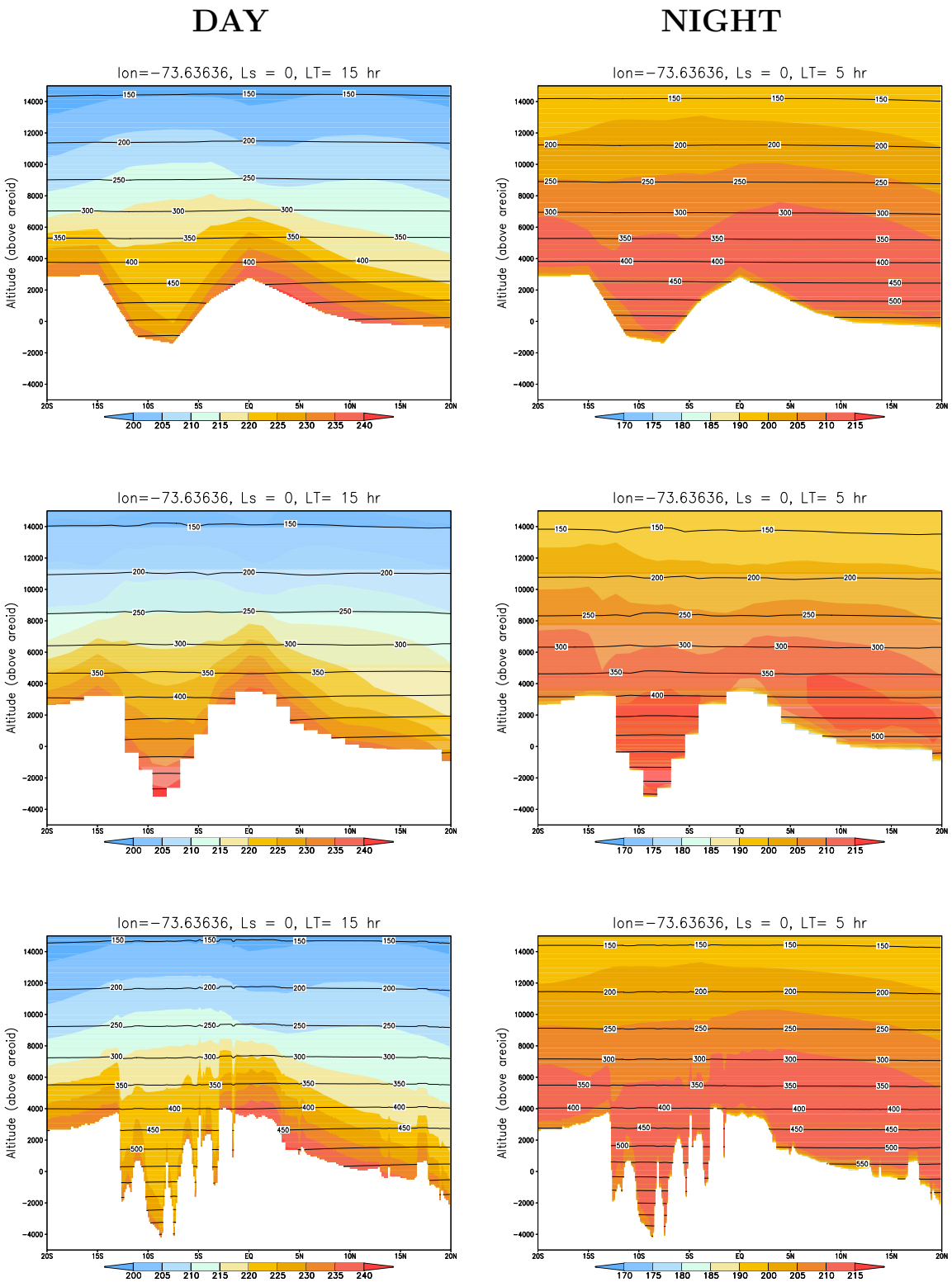

Figure 19: Cross-section of temperature fields (colored) and pressure level (black contour) near Valles Marineris from MCD V4.2 at GCM resolution (top row), from a high resolution 176×132 GCM (middle row), and from the high resolution output of MCD V4.2. Note that there is an order of magnitude between horizontal and vertical scales in these plots; what appear as sharp gradients in the horizontal direction are in fact quite smooth when displayed using more commensurate axes.

A Computing Martian Dates and Local Time

In this appendix we briefly describe how one may compute aerocentric solar longitude of Mars for a given Julian date, as well as how to compute corresponding Local True Solar Time.
The equations and methods given here are taken from Capderou (2005) which should be consulted for a detailed description.

A.1 Some constants

	88775.245	Number of seconds in a sol (martian day)
N_s	668.6	Number of sols in a martian year
Ls_{peri}	250.99	Perihelion date (in deg.)
t_{peri}	485.35	Perihelion date (in sols)
a	1.52368	Semi-major axis of orbit (in AU)
e	0.09340	Orbital eccentricity
ϵ	25.1919	Obliquity of equator to orbit (in deg.)

A.2 Computing martian dates and aerocentric solar longitude

A.2.1 The three anomalies

For an elliptical trajectory, the **true anomaly** ν is given by the polar angle of the position, with the convention that $\nu = 0$ at the periastron (minimum distance to center, i.e. the perihelion, in Mars' case).

If $n = 2\pi/T$ is the mean angular frequency of motion (T is the period of revolution, i.e. a year), then at time t (taking the time origin as $t = t_{peri}$, perihelion date at which $\nu = 0$):

$$n(t - t_{peri}) = 2 \arctan\left[\sqrt{\frac{1-e}{1+e}} \tan\frac{\nu(t)}{2}\right] - \frac{e\sqrt{1-e^2}\sin\nu(t)}{1+e\cos\nu(t)} \tag{30}$$

The **eccentric anomaly** E is related to mean motion n by:

$$n(t - t_{peri}) = E(t) - e\sin E(t) \tag{31}$$

The **mean anomaly** M is the angle determining the position of a fictitious point in uniform circular motion of angular frequency n. Thus,

$$n(t - t_{peri}) = M(t) \tag{32}$$

A.2.2 Aerocentric solar longitude Ls

The position of the planet on its heliocentric orbit is given by the aerocentric solar longitude Ls. The origin of Ls is defined as the vernal equinox (northern hemisphere spring equinox).

Ls is directly related to the true anomaly ν:

$$\nu = Ls - Ls_{peri} \tag{33}$$

where Ls_{peri} is the perihelion date.

A.2.3 Converting Julian date JD to Martian sol number D_s

For a given Julian date JD, the corresponding martian sol date $D_s \in [0; N_s]$ (i.e. number of sols elapsed since beginning of martian year defined by $Ls = 0$):

$$D_s = (JD - JD_{ref})\frac{86400}{88775.245} \ (mod\, N_s) \tag{34}$$

where 86400 and 88775.245 are respectively the number of seconds in an earth day and a martian sol. JD_{ref} is a reference Julian date corresponding to an $Ls = 0$ event.
Example of reference date: $Ls = 0$ occurred on 19-12-1975 at 4:00:00, which corresponds to Julian date 2442765.667.

A.2.4 Converting sol number D_s date to Ls

For a given sol number $D_s \in [0; N_s]$, the corresponding value of aerocentric solar longitude Ls may be computed as follows:

Step1: Compute mean anomaly $M(D_s)$ (in radians):

$$M = 2\pi\frac{D_s - t_{peri}}{N_s} \tag{35}$$

Step 2: Compute eccentric anomaly $E(D_s)$ (in radians):
This is the tricky bit (also known as Kepler's problem). Eccentric and mean anomalies are related by the nonlinear equation:

$$M = E - e\sin E \tag{36}$$

which must be solved by, for instance, a Newton iterative procedure.
Step 3: Compute true anomaly $\nu(D_s)$ (in radians) using:

$$\nu = 2\arctan\left[\sqrt{\frac{1+e}{1-e}}\tan\left(\frac{E}{2}\right)\right] \tag{37}$$

Step 4: Compute $Ls(D_s)$ (in degrees):

$$Ls = \left(\nu\frac{180}{pi} + Ls_{peri}\right) \ (mod\, 360) \tag{38}$$

A.3 Computing Local True Solar Time

The steps required to compute the Local True Solar Time at a given longitude lon (in degrees East) for a given Julian Date are the following:
Step 1: Compute Local Mean Time LMT_0 at longitude 0, in martian hours, for a given Julian date JD :

$$LMT_0 = \left(LMT_{ref} + 24(JD - JD_{ref})\frac{86400}{88775.245}\right)(mod\, 24) \tag{39}$$

Where JD_{ref} is a reference Julian date, and LMT_{ref} the Local Mean Time at longitude 0, in martian hours, at that date. 86400 and 88775.245 are respectively the number of seconds in an earth day and a martian sol.
Example of reference date and time: 01-01-1976 at 00:00:00 was such that $JD_{ref} = 2442778.5$ and $LMT_{ref} = 16.1725$.

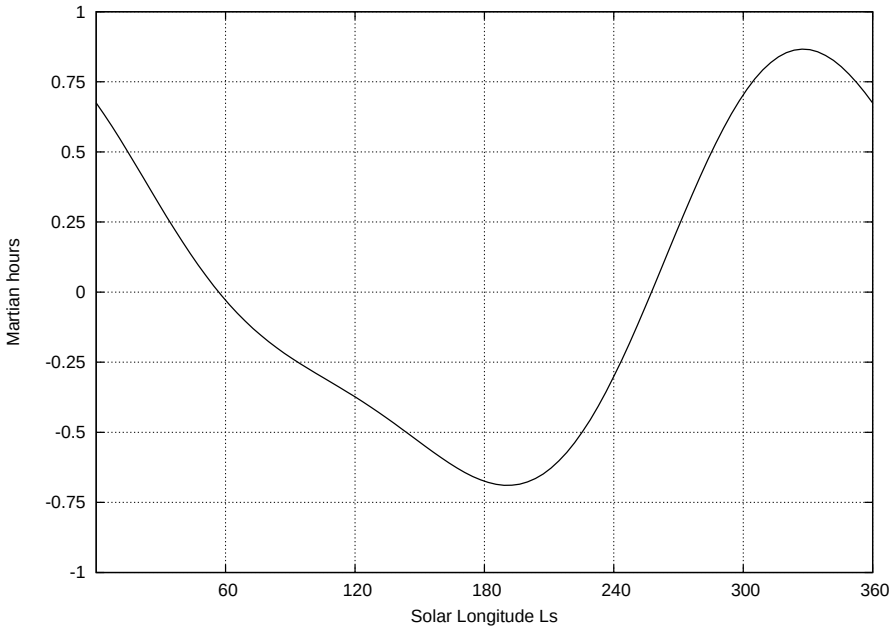

Figure 20: Equation Of Time (EOT) for Mars, showing the difference between Mean Local Time and True Solar Time, as a function of Solar Longitude Ls.

Step 2: For the given aerocentric solar longitude Ls (which is obtained from Julian Date JD as explained previously), compute the Equation Of Time EOT (which yields, in martian hours, the difference between Mean Time and True Solar Time; see Figure 20) :

$$EOT = \left[2e\sin\left(Ls - Ls_{peri}\right) - \tan^2\left(\frac{\epsilon}{2}\right)\sin\left(2Ls\right)\right]\frac{24}{2\pi} \tag{40}$$

Where Ls_{peri} is the perihelion date, e the orbital eccentricity and ϵ the obliquity of equator to orbit.

Step 3: Compute Local True Solar Time at longitude 0, $LTST_0$, in martian hours:

$$LTST_0 = LMT_0 - EOT \tag{41}$$

step 4: At longitude lon (in degrees east), Local True Solar Time $LTST$, in martian hours, is then:

$$LTST = \left(LTST_0 + \frac{lon}{15}\right)(mod\,24) \tag{42}$$

B References

Banks, P.M. and G. Kockarts, 1973, *Aeronomy, part A*, Academic Press, New York.
Capderou M. (2005) *Satellites Orbits and Missions*, Springer.
Collins, M. and Lewis, S.R. (1997a) *Mars Climate Database v1.0: User Manual,* European Space Agency Technical Report.
Collins, M. and Lewis, S.R. (1997b) *Mars Climate Database v1.0: Detailed Design Document,* European Space Agency Technical Report.
Collins, M., Lewis, S.R., Read, P.L., Thomas, N.P.J., Talagrand, O., Forget, F., Fournier, R., Hourdin, F. and Huot, J.-P. (1996) "A climate database for the Martian atmosphere,"

in *Environment Modelling for Space-based Applications*, European Space Agency **SP–392,** 323–327.
Collins, M., Lewis, S.R. and Read, P.L. (1997) "Gravity wave drag in a global circulation model of the Martian atmosphere: Parameterisation and validation," *Adv. Space Res.,* **19,** 1245–1254.
Forget, F., Hourdin, F., Fournier, R., Hourdin, C., Talagrand, O., Collins, M., Lewis, S.R., Read, P.L. and Huot, J.-P. (1999) "Improved general circulation models of the Martian atmosphere from the surface to above 80 km," *J. Geophys. Res.,* **104,** 24,155–24,176.
Forget, F., C. Hourtolle, and Lewis, S.R. (2000a) *Mars Climate Database atmemcd subroutine prgrammer's guide.*
González-Galindo, F., López-Valverde, M. A., Angelats i Coll, M. and Forget, F. (2005) "model to thermospheric altitudes: UV heating and photochemical modules," JGR 110, doi:10.1029/2004JE002312.
Hourdin, F., Le Van, P., Forget, F. and Talagrand, O. (1993) "Meteorological variability and the annual surface pressure cycle on Mars" *J. Atmos. Science* **50**, 3625–3640.
Hourtolle, C., Forget, F. and Lewis, S.R. (2000b) *Mars Climate Database "atmemcd" subroutine programmer's reference.*
Justus, C.G. (1990) "A Mars Global Reference Atmosphere Model (Mars-GRAM) for mission planning and analysis," *AIAA Paper No. 90–0004,* 28th Aerospace Sciences Meeting.
Justus, C.G., Alyea, F.N., Cunnold, D.M., Jeffries, W.R. III, and Johnson, D.L. (1995) "The NASA/MSFC Global Reference Atmosphere Model – 1995 Version (GRAM-95)," *NASA Technical Memorandum.*
Lean, J.L. (1987) "Solar UV irradiance variations: a review," JGR 92, 839-868.
Lean, J.L. (1991) "Variations in the Sun's radiative output," Rev. Geophys., 29, 505-535.
Lean, J.L. et al. (2001) "Variability of a composite chromospheric irradiance index during the 11-year activity cycle and over longer time periods," JGR 106, 10645-10658.
Lemoine, F.G., Smith, D. E., Rowlands, D. D., Zuber, M. T., Neumann, G. A., and Chinn, D. S. (2001) "An improved solution of the gravity field of Mars (GMM-2B) from Mars Global Surveyor," *J. Geophys. Res,* 106(E10), 23359-23376.
Lewis, S.R. and Collins, M. (1999a) *Mars Climate Database v2.0: User Manual,* European Space Agency Technical Report.
Lewis, S.R. and Collins, M. (1999b) *Mars Climate Database v2.0: Detailed Design Document,* European Space Agency Technical Report.
Lewis, S.R., Collins, M. and Forget, F. (2000a) *Mars Climate Database v2.3: User Manual,* European Space Agency Technical Report.
Lewis, S.R., Collins, M. and Forget, F. (2000b) *Mars Climate Database v2.3: Detailed Design Document,* European Space Agency Technical Report.
Lewis, S.R., Collins, M. and Forget, F. (2001a) *Mars Climate Database v3.1: User Manual,* European Space Agency Technical Report.
Lewis, S.R., Collins, M. and Forget, F. (2001b) *Mars Climate Database v3.1: Detailed Design Document,* European Space Agency Technical Report.
Lewis, S.R., Collins, M., Forget, F., Wanherdrick, Y. and Bingham, S.J. (2004a) *Mars Climate Database v3.2: User Manual,* European Space Agency Technical Report.
Lewis, S.R., Collins, M., Read, P.L., Forget, F., Hourdin, F., Fournier, R., Hourdin, C., Talagrand, O. and Huot, J.-P. (1999) "A Climate Database for Mars," *J. Geophys. Res.,* **104,** 24,177–24,194.
Lewis, S.R., Read, P.L., Conrath, B.J., Pearl, J.C. and Smith, M.D. (2007) "Assimilation of Thermal Emission Spectrometer atmospheric data during the Mars Global Surveyor aerobraking period," *Icarus,* doi: 10.1016/j.icarus. 2007.08.009
Millour, E., Forget, F. and Lewis, S.R. (2007) *Mars Climate Database v4.2: User Manual,* European Space Agency Technical Report.

Mo, K.C., and Ghil, M. (1987) "Statistics and dynamics of persistent anomalies," *J. Atmos. Sci.,* **55,** 877–901.
Montabone, L., Lewis, S.R., Read, P.L. and Hinson D.P. (2006) "Validation of martian meteorological data assimilation for MGS/TES using radio occultation measurements," *Icarus,* doi: 10.1016/j.icarus.2006.07.012
North, G.R. (1984) "Empirical Orthogonal Functions and Normal Modes," *J. Atmos. Sci.* **41,** 879–887.
Read, P.L., Collins, M., Forget, F., Fournier, R., Hourdin, F., Lewis, S.R., Talagrand, O., Taylor, F.W. and Thomas, N.P.J. (1997) "A GCM climate database for Mars: For mission planning and for scientific studies," *Adv. Space Res.* **19,** 1213–1222.
Seidelmann, P. K., Abalakin, V. K., Bursa, M., Davies, M. E., de Bergh, C., Lieske, J. H., Oberst, J., Simon, J. L., Standish, E. M., Stooke, P. and Thomas, P. C. (2002) "Report of the IAU/IAG Working Group on Cartographic Coordinates and Rotational Elements of the Planets and Satellites: 2000" *Cel. Mech. Dyn. Astron.,* **82,** 83–110.
Spiga, A., Forget, F., Dolla, B., Vinatier, S., Melchiorri, R., Drossart P., Gendrin, A., Bibring, J., Langevin, Y. and Gondet, B. (2007) "Remote sensing of surface pressure on Mars with the Mars Express/OMEGA spectrometer: 2. Meteorological maps", *J. Geophys. Res.,* **112, E08S16,** doi:10.1029/2006JE002870
Woods, T.N. et al. (2004) "Solar extreme ultraviolet and X-ray irradiance variations, in Solar variability and its effect on climate," Geophys. Monogr. Ser., vol. 141, ed. J. Pap et al.